POLITEHNICA UNIVERSITY OF BUCHAREST
MATERIAL SCIENCE AND ENGENEERING FACULTY
DOCTORAL SCHOOL OF MATERIALS SCIENCE AND ENGINEERING

Ph.D. THESIS ABSTRACT

Prediction and optimizing advanced nickel-base superalloys features by computational methods

Ph.D. Supervisor: Prof. Dr. Eng. Mihai Ovidiu COJOCARU
Author: Eng. Mihaela Raluca CONDRUZ

Ph.D. Evaluation Board

President	Prof.habil dr.ing. Iulian Vasile ANTONIAC	de la	Politehnica Univ. of Bucharest
Ph.D. supervisor	Prof.dr.ing. Mihai Ovidiu COJOCARU	de la	Politehnica Univ. of Bucharest
Referent	Prof.dr.ing. George ARGHIR	de la	Technical Univ. of Cluj Napoca
Referent	Prof.dr.ing. Ioan GIACOMELLI	de la	„Transilvania” Univ. of Brașov
Referent	Conf.dr.ing. Mihai BRÂNZEI	de la	Politehnica Univ. of Bucharest

BUCHAREST
2020

TABLE OF CONTENTS

*T – thesis

**A – abstract

Key words: additive manufacturing, Ni-base superalloys, SLM, computational, CAFÉ, CALPHAD, phase prediction, characteristics optimization, volumetric energy density, isothermal oxidation, segregation, recirculated powder, microstructure, scanning strategy

ACKNOWLEDGEMENT

On the occasion of completing my Ph.D. I would like to express my gratitude to the people who helped and supported me throughout the course and to the realization of this thesis.

First of all, I would like to thank the Ph.D. supervisor, Prof. Dr. Eng. Mihai Ovidiu COJOCARU from the Politehnica University of Bucharest, Faculty of Materials Science and Engineering, Department of Metallic Materials Science, Physical Metallurgy, for the support provided during the years of study and writing the thesis.

My deepest gratitude to the Scientific Director of the National Research and Development Institute for Gas Turbines COMOTI, Dr. Eng. Gheorghe MATACHE, both for the guidance provided during the research and writing of this thesis and for the material support provided, without it the research would not have been possible. Special thanks to Dr. Eng. Cristian PUȘCAȘU, from the National Research and Development Institute for Gas Turbines COMOTI, Department of Gas Turbines Special Components. Physical and mechanical testing laboratory, for the support provided for the entire Ph.D. period.

I would also like to thank my colleagues from the Department of Gas Turbines Special Components. Physical and mechanical testing laboratory both for the assistance during the experimental research and for the moral support: Eng. Alexandru PARASCHIV, Eng. Tiberius FRIGIOESCU, Eng. Teodor BADEA, Ec. Andreea DEUTSCHLANDER, Dr. Eng. Adina TOMA, Eng. Mihaela GRIGORESCU, Techn. Dănuț ANTONESCU.

I would like to thank my family for the encouragement, support, and patience they have shown throughout the Ph.D. period.

Thank you for the financial support provided by the projects carried out within the National Research and Development Institute for Gas Turbines COMOTI:

- „Assessments to Prepare and De-Risk Technology Developments - Developing Metal Additive Manufacturing Expertise to meet the Requirements of Space Industry”, acronym SPARk, contract no. 4000126703/19/NL/BJ/va funded by European Space Agency – ESA;
- 2018 Nucleu Programme, project „Cercetări teoretice și experimentale privind mecanismele de răspuns a materialelor anizotrope la solicitări termice și/sau mecanice”, contract no. 7N/2018 (Programme Title: „Cercetări teoretice și experimentale pentru creșterea performanțelor sistemelor de propulsie aeriene și terestre”, acronym TURBO 2020+) funded by Minstry of Research and Innovation;
- 2019-2022 Nucleu Programme, project „Cercetări teoretice și experimentale privind optimizarea performanțelor materialelor refractare, rezistente la temperaturi ridicate, realizate prin procese inovative”, contract no. 2N/2019 (Programme Title: „Cercetări avansate asupra sistemelor de propulsie și mașinilor paletate rotative, acronym TURBOPROP) funded by Ministry of Education and Research.

INTRODUCTION

The present thesis addresses two areas of interest for the scientific and industrial community, namely the prediction and optimization of the characteristics of nickel-based superalloys through computational methods and their manufacture by advanced technologies.

Currently, worldwide the researches in the material science field focus on the characterization of additive manufactured materials to validate and integrate this technology in leading industrial fields, such as aerospace and aeronautics. Although the first additive manufacturing method was developed in the 1980s and subsequently multiple methods were developed, its integration in these fields was not possible because the limitations induced by this technological process were not overcome.

The main challenges identified in the case of additive manufacturing technology of metal products are related to the quality and integrity of the resulting material, aiming to obtain materials characterized by a high level of densification simultaneously with a reduced anisotropic degree. To achieve these goals, the world's scientific communities are investing more and more in the field of metal additive manufacturing research. This fact was proved by the upward technology evolution. Forecasts regarding the additive manufacturing products and services were provided by the 2019 Wohlers Report, they forecast that the additive market will reach $ 15.8 billion by 2020, $ 23.9 billion by 2022, respectively $ 35.6 billion by 2024.

Globally, the research in the field of additive manufacturing is limited to a reduced number of metallic materials, due to the production costs of raw material and the fact that not all metallic materials are suitable for this technology. Moreover, given the general costs involved in making a product by metal additive manufacturing, the use of this technology is only justified if the product is characterized by high complexity and cannot be produced by other conventional manufacturing methods. Generally, the products intended for additive manufacturing are prototypes, unique parts, or intended for top fields.

Metallic materials used for additive manufacturing include Ni-based superalloys. This category of alloys is characterized by the fact that it can withstand mechanical stresses during operation in extreme environments (at high temperatures, in corrosive/oxidizing environments). Until relatively recently, Ni-based superalloys products were manufactured using conventional processes such as forging (forged superalloys), conventional casting (superalloys with an equiaxed crystal structure), directional casting and solidification (superalloys with columnar or monocrystalline structure), and methods specific to powder metallurgy (sintered superalloys).

In the last two decades, researches have been directed towards the production of superalloy products by additive manufacturing technology through methods that use metal powders as raw material. Additive manufactured metallic materials stand out by the manufacturing process induced characteristics, presenting superior mechanical characteristics to materials manufactured by conventional methods. Researches in the field have led to a large number of factors that can significantly influence the characteristics of additively manufactured metallic materials, from the properties of the raw material to multiple process parameters and the post-processing conditions.

In the current context, the thesis scientific research activity was directed to the additive manufactured Ni-base superalloy, IN 625, intended for gas turbine engine components. Based on the fact that nowadays, new product development without computer-aided planning and calculation methods is not possible, and computational methods have been developed to predict different characteristics of products manufactured by conventional methods, the need to study the capabilities of computer models adapted to additive manufactured products is justified. These statements underlie the general objective of the thesis.

The general objective of the thesis was to integrate into an innovative way, analytical and thermodynamic calculations based on the CALPHAD method in case of the IN 625 superalloy, with tools based on the cellular automaton finite element model (CAFE) adapted to additive materials for prediction and optimizing its microstructural characteristics, with experimental research.

Given the current state of the art in the field of additive manufactured Ni-based superalloys, to achieve the general objective of the thesis, several specific objectives have been established:

1. to ascertain the characteristics of the raw material used for the additive manufacturing process and to determine the influence of the recirculation process on its characteristics;
2. prediction and optimizing the microstructural characteristics of the additive manufactured IN 625 by computational methods;
3. experimental validation of the results obtained by computational methods;
4. determination of the volumetric energy density influence on the densification degree of the SLM manufactured IN 625;
5. determination of the microstructural anisotropy influence on the tensile characteristics of additively manufactured IN 625;
6. evaluation of high-temperature oxidation behavior of SLM manufactured IN 625.

To achieve the objectives, a research methodology was developed, which integrates new and varied methods, techniques, and programs applied for predicting, optimizing, and characterizing the IN 625 manufactured by an advanced method, typical to additive manufacturing technology. The results obtained by computational methods were compared with experimental results obtained during the Ph.D. period and with results obtained by other researchers.

CHAPTER 1. GENERAL ASPECTS REGARDING THE METAL POWDER ADDITIVE MANUFACTURING

Chapter 1 presents the state of the art in the field of metal powder additive manufacturing technology. In this chapter are described the methods specific to additive manufacturing technology, the limitations of the selective laser melting method (applied in experimental research), is presented the state of the art in the field of Ni-based superalloys for additive manufacturing, but also the state of the art in the field of computational methods used internationally for predicting the characteristics of additively manufactured metallic materials.

CHAPTER 2. METHODS AND EQUIPMENT USED FOR MANUFACTURING AND CHARACTERIZATION OF ADDITIVE MANUFACTURED IN 625 SUPERALLOY

Chapter 2 presents the software, materials, methods, and equipment used to perform the computational and experimental research. The goal of the thesis was to conduct computational and experimental research in the field of metal powder additive manufacturing of IN 625 material.

The experimental research was initiated with the study of the raw material characteristics and their evolution over time. Afterward, it was proceeded with the study of the SLM manufactured material's properties, combining computational methods using Pandat^{TM} and ANSYS Additive Suite software, Additive Science module (Microstructure) with experimental research performed on additively manufactured IN 625 using Lasertec 30 SLM equipment produced by DMG MORI and powder purchased from LPW Technology Ltd.

The experimental researches were focused on analyzing the microstructure development, phase development, and the influence of process parameters on the material's properties. Figure 2.13 shows the research plan.

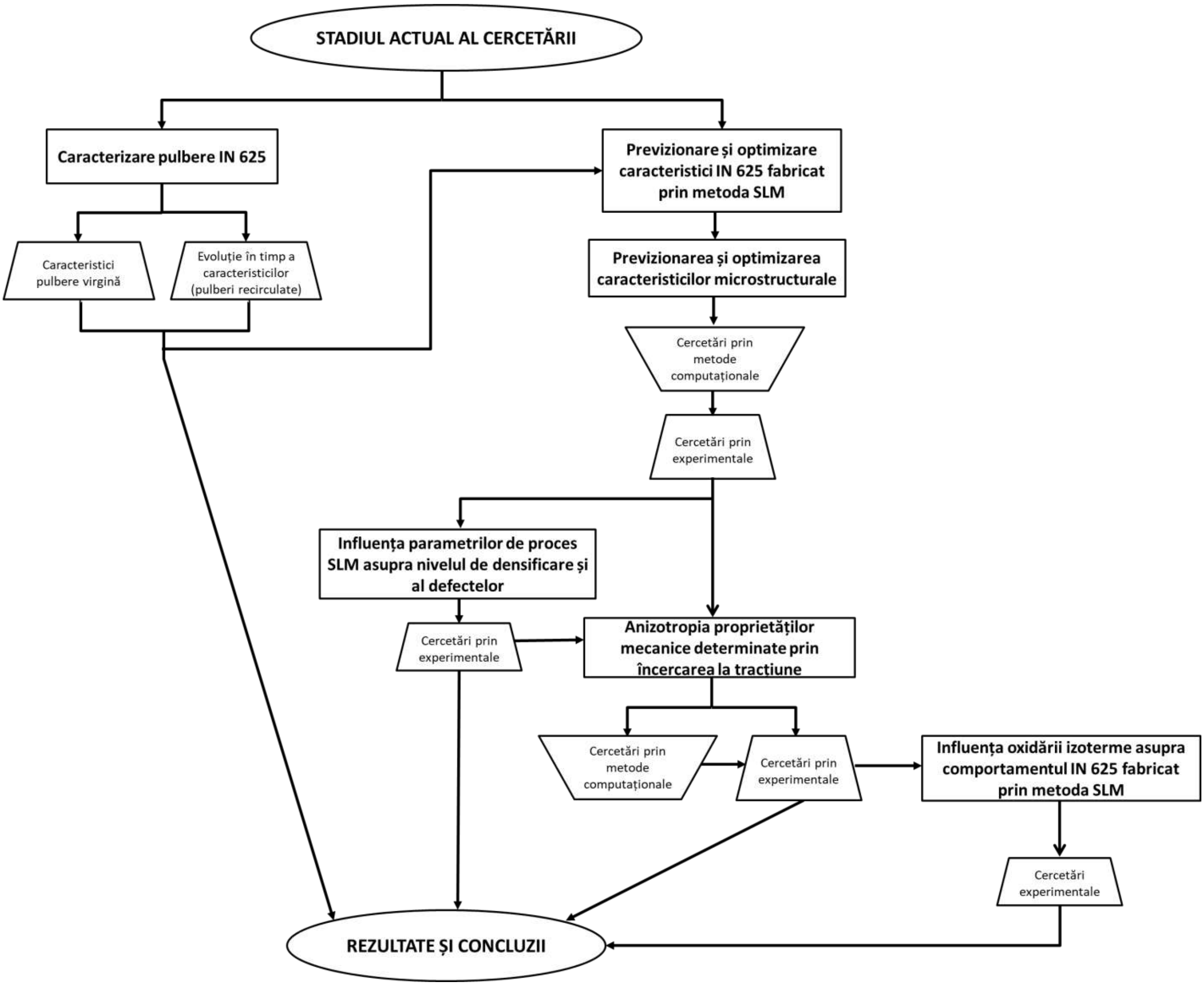

Figure 2.13. Research flowchart

CHAPTER 3. EXPERIMENTAL RESEARCH

3.1 Experimental research on IN 625 powder and the evolution of its characteristics over time

The characteristics of the powder lot UK81572, used to additive manufacture all specimens, were measured to achieve the research's goal. The characteristics were determined both at the time of the acquisition, before starting of the experiments (virgin powder characteristics), and after their use and recirculation (recirculated powders characteristics).

The powder characteristics were monitored over 17 months, when were performed multiple manufacturing cycles, according to the data presented in Table 3.1. At the end of the 17 months, it was estimated that the powder was recirculated approximately 26 times.

Table 3.1. Powders used for research

Powder type	Cod	Observații
Virgin powder	V	-
Recirculated powder	R1	Sampled after 4 manufacturing cycles were performed
	R2	Sampled after 19 manufacturing cycles were performed
	R3	Sampled after 28 manufacturing cycles were performed
	R4	Sampled after 37 manufacturing cycles were performed
	R5	Sampled after 48 manufacturing cycles were performed
	R6	Sampled after 95 manufacturing cycles were performed

The powder characteristics that were determined were:

- Physical properties:
    - Powder particles' morphology;
    - Powder particles' surface quality;
    - Powder particles' dimensional evolution;
    - Powder size distribution;
- Technological properties:
    - Apparent density;
    - Tapped density;
    - Rheological properties – determined based on powder flowability determined by measuring the powder flow rate, the Hausner ratio, Carr index and angle of repose.

Experimentally, it was found that the virgin powder falls within the particle size range specified by the technical specification and complies with the recommendations of the Lasertec 30 SLM equipment manufacturer. However, as the powder was recirculated, the particle size range D_{90}, D_{50}, and D_{10} narrowed, which shows that during each manufacturing process, the number of particles at the upper limit of the particle size range decreases, these particles being either molten or covered with splashes of molten material (forming satellite particles) and can no longer pass through the mesh of the equipment's sieve.

These results are consistent with the results obtained by other authors who have conducted studies on the characteristics of metal powders for additive manufacturing, before and after their recycling [126, 129, 240, 241].

Although there has been a decrease in the mean values D_{90}, D_{50}, and D_{10} of the powder size range, it is not significant. The D_{90} value decreases only by 10% compared to the value registered in the case of the virgin powder, respectively 5% compared to the minimum value recommended by the equipment manufacturer DMG MORI.

The morphology of virgin powder particles is typical to powders obtained by metal melting in a vacuum furnace followed by gas atomization. The majority of particles are characterized by a regular spherical morphology, with a smooth surface, but also by spherical particles with satellites resulting from the gas atomization process (Figure 3.4).

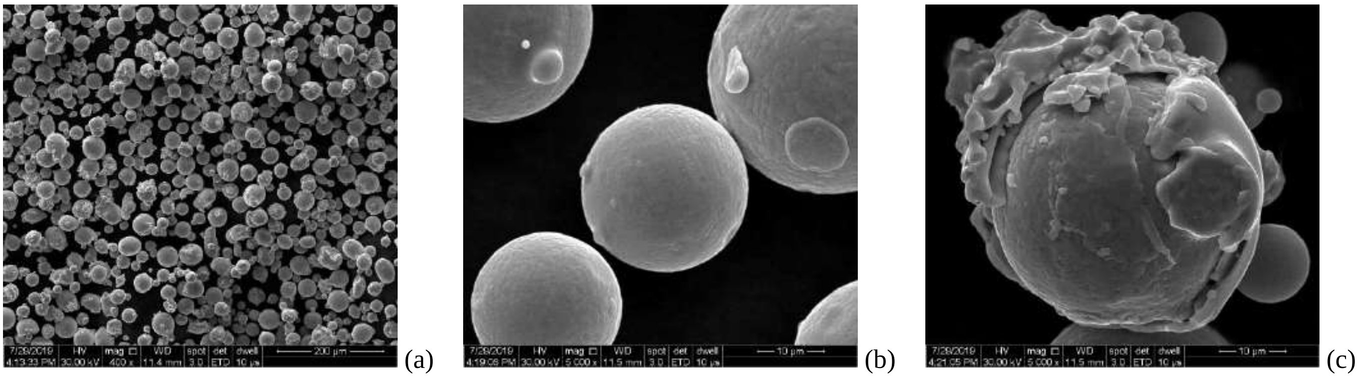

Figure 3.4. SEM representative images with the IN 625 virgin powder particles a) powder particles – magnification 400x; b) spherical powder particle – magnification 5000x; c) spherical powder particle with satellites – magnification 5000x

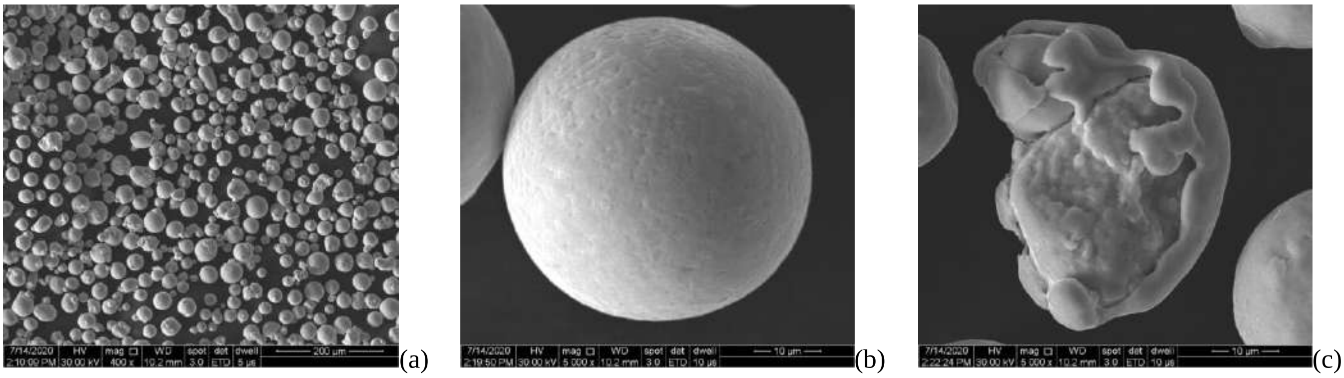

Figure 3.5. SEM representative images with the IN 625 recirculated powder particles a) powder particles – magnification 400x; b) spherical powder particle – magnification 5000x; c) spherical powder particle with satellites – magnification 5000x

Based on the analysis performed on SEM images it was found that there are no significant differences between the morphology of the virgin powder particles and that of the recirculated powder particles. The recirculated particles are characterized by a spherical morphology, but there were also observed particles with satellites formed either from gas atomization or from the detachment of splashes from the melt pool during the SLM process (Figure 3.5). In addition to these satellite particles, elongated particles were also observed. The dimensional analysis of the powders showed that both the virgin powder particles and the recirculated powder particles show deviations from the ideal circularity, deviations more pronounced after multiple recirculation stages.

The recirculated powders have higher values of both the apparent and tapped density compared to the virgin powders, this may be caused by the morphology of the powder particles. Besides, in the case of recirculated powders, many small particles (<10 μm) were observed – solidified spatter that covers the voids between larger particles.

Similar to density, an increase in HR and C values was identified as the powder is recirculated, but the calculated values are in the accepted ranges found in the literature (HR <1.25; C <15), indicating that the powders do not present very high cohesive forces but have a good capacity to form compact layers.

No significant differences were observed in the flow rate of virgin and recirculated powders, both types of powder have values of approximately 8 s / 150g (± 0.2 s) values according to the technical specification of the powder (<10 s / 150 g). The natural slope angle determined for the two types of powder has values below 40°, which indicates a good flow capacity of the powder [121].

3.2 Microstructural development in additive manufactured IN 625 by SLM

3.2.1 Crystallization of the superalloy

The microstructure of additively manufactured IN 625 developed following the heterogeneous germination at the powder particles/support material - melt pool interface and crystals grow along the highest thermal gradient direction. The growth process is completed after the growth of all germs from the last added layer. Due to a high ratio between the undercooling and high solidification rate, the structure developed in the additive manufactured IN 625 has a cellular morphology in some areas and a dendritic morphology in other areas. Microstructural details can be observed in the scattered electrons SEM images shown in Figure 3.12, but also in the optical microscopy images shown in Figure 3.13.

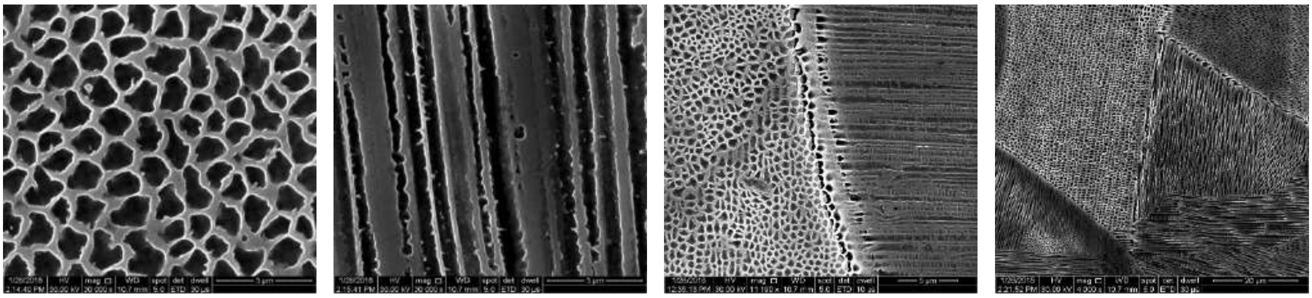
(a) (b) (c) (d)

Figure 3.12. SEM images with microstructural details of the microstructure of SLM manufactured IN 625 in as-built state: a) cellular structure; b) dendrite; c) heat affected zone (HAZ) that separates two layers; d) microstructure with cellular and columnar morphology

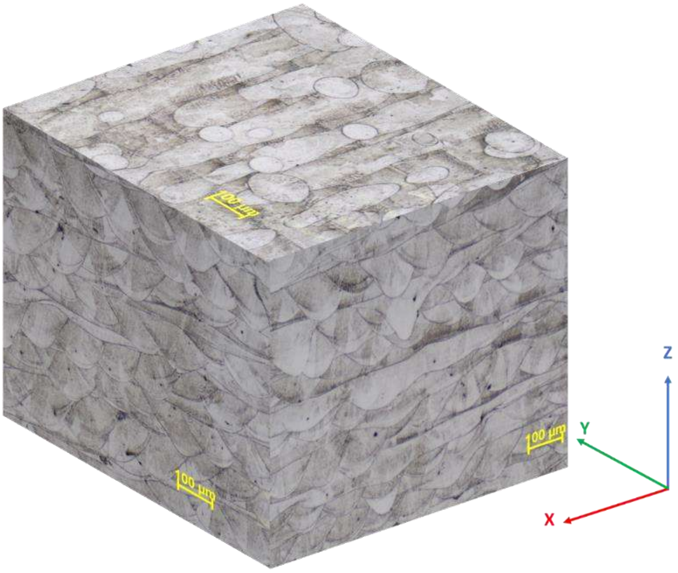

Figure 3.13. 3D representation of microstructural characteristics of SLM manufactured IN 625 in as-built state (magnification 100x)

The microstructure of the additive manufactured IN 625 is similar to the welded parts microstructure; the layer boundaries and the HAZ (also found in welded structures) can be observed. In the optical microscopy images, the deposited layers that can be observed in the YOZ and XOZ planes, they are similar to the fish scales welding microstructure, while on the XOY plane, the laser path and the melt pool trace can be observed.

3.2.2 Analysis of the compositional variation influence on transformation temperatures and phase development

The thermodynamic calculations were performed to determine the influence of the main alloying elements composition from IN 625 on the transformation temperatures and phase development. The research was performed using the Pandat™ software (Computherm LLC.) with the PanNi2020_TH database (from the National Research and Development Institute for Gas Turbines COMOTI), a program based on the CALPHAD method.

By changing the concentration of the alloying elements in the range accepted by the standard for the IN 625 superalloy, according to the matrix with three factors and three levels applied (matrix 3^3, Cr = 20 - 23%wt., Mo = 8 - 10%wt., Nb = 3.15 - 4.15%wt., where 0 is the minimum concentration of the element, 1 is the average concentration of the element, 2 is the maximum concentration of the element), the liquidus temperature changes. This temperature is in the range of 1392.2 ° C - 1377.6 ° C (14.6 °C), and the liquidus temperature values calculated according to the predefined matrix are presented in Table 3.5.

Not only the liquidus temperature is influenced by the concentration of the three alloying elements, but they also have a significant influence on the solidus temperature. The solidus temperature varies between 1350.5 ° C - 1323 ° C (27.5 ° C), according to the data presented in Table 3.6.

Table 3.5. Cr, Mo, Nb concentration influence on liquidus temperature

Mo	Nb	Cr		
		0	1	2
0	0	**1392,2°C**	1389,3°C	1386,3°C
0	1	1388,0°C	1385,1°C	1382,0°C
0	2	1383,8°C	1380,8°C	1377,7°C
1	0	1392,1°C	1389,2°C	1386,2°C
1	1	1387,8°C	1385,0°C	1382,0°C
1	2	1383,5°C	1380,7°C	1377,7°C
2	0	1391,8°C	1389,1°C	1386,2°C
2	1	1387,6°C	1384,8°C	1381,9°C
2	2	1383,3°C	1380,5°C	**1377,6°C**
	IN 625 (SLM)		**T_L = 1386°C**	

Table 3.6. Cr, Mo, Nb concentration influence on solidus temperature

Mo	Nb	Cr		
		0	1	2
0	0	**1350,5°C**	1346,3°C	1341,9°C
0	1	1342,2°C	1337,9°C	1333,4°C
0	2	1333,8°C	1329,4°C	1325,0°C
1	0	1349,5°C	1345,3°C	1341,1°C
1	1	1341,1°C	1336,8°C	1332,6°C
1	2	1332,6°C	1328,3°C	1324,0°C
2	0	1348,5°C	1344,4°C	1340,3°C
2	1	1339,9°C	1335,8°C	1331,6°C
2	2	1331,3°C	1327,2°C	**1323,0°C**
	IN 625 (SLM)		**T_S = 1339°C**	

The values obtained for the liquidus and solidus temperatures are close to the values obtained experimentally by Cieslak et. al. [247] for various compositional ranges of the alloy IN 625 manufactured by conventional methods. Regarding the thermodynamic calculations performed for the specific chemical composition of the material used for additive manufacturing, a liquidus temperature of T_L = 1386°C and two solidus temperatures were predicted, one for solidification under equilibrium conditions (T_S = 1339°C), respectively a much underestimated one related to the solidification in non-equilibrium conditions (T_S = 1195°C) - Figure 3.23.

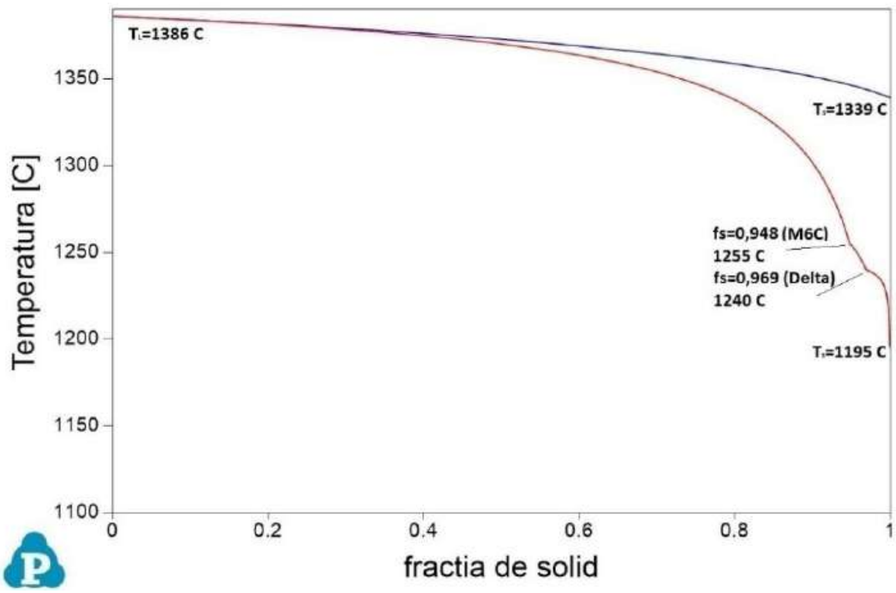

Figure 3.23. Solidification path in equilibrium and non-equilibrium conditions determined based on the chemical composition of the IN 625 alloy used for additive manufacturing

Also, the formation of the γ phase was predicted, followed by the δ phase (at a solid fraction fs = 0.969, respectively T = 1240ºC) and the primary carbides of M_6C type (at fs = 0.948, respectively T = 1255ºC). An advantage of the Scheil method used to predict the solidification of the alloy is that it allows the analysis of how the alloying elements are redistributed in the solidification front (Figure 3.24).

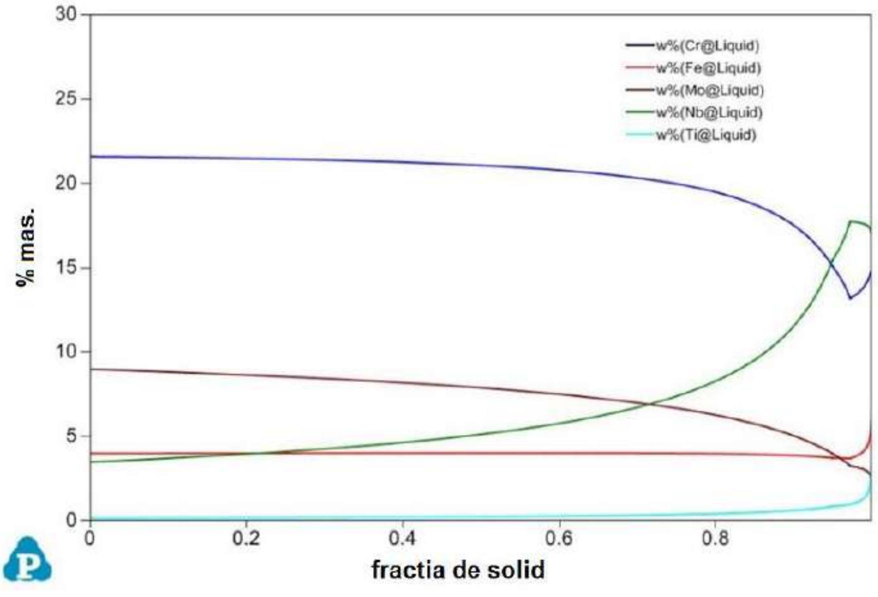

Figure 3.24. Prediction of the alloying elements redistribution in the solidification front

The diagram that shows the prediction of the redistribution of the alloying elements in the solidification front shows that Nb has the highest tendency of redistribution in the liquid phase, hence preferentially segregating in the interdendritic spaces at the end of the solidification process.

To confirm this hypothesis, compositional analyses were performed by EDS in microvolumes in an area with cellular structure. The determinations were performed both in the center of the cells and the intercellular area (Figure 3.25). Based on the average chemical compositions acquired, the partition coefficient Ks was calculated for the main elements identified for this superalloy (Table 3.8).

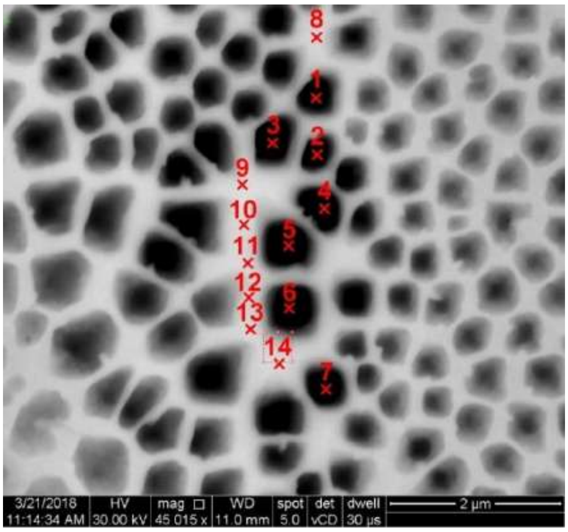

Figure 3.25. Microvolumes of EDS quantitative analysis in cellular areas and in intercellular spaces

Table 3.8. Alloying elements concentration in cellular and intercellular areas

	Chemical composition, [%wt.]						
Point	Nb	Mo	Ti	Cr	Fe	Co	Ni
1	2.55	6.73	0.17	22.36	3.86	0.1	64.12
2	2.25	5.86	0.17	22.41	3.76	0.11	65.34
3	2.56	6.94	0.16	22.3	3.9	0.11	63.9
4	3.14	7.49	0.17	22.15	3.88	0.11	62.9
5	2.43	6.06	0.17	22.5	4.04	0.1	64.58
6	2.36	6.35	0.17	22.29	3.91	0.11	64.69
7	2.97	7.5	0.18	21.88	3.96	0.11	63.27
Average	**2.61**	**6.70**	**0.17**	**22.27**	**3.90**	**0.11**	**64.11**
8	4	9.53	0.17	21.42	3.72	0.1	60.84
9	4.39	10.21	0.17	21.11	3.76	0.1	60.04
10	4.27	10.64	0.16	20.77	3.66	0.09	60.13
11	3.99	9.53	0.18	21.15	4	0.1	60.84
12	3.72	9.21	0.17	21.75	3.97	0.1	60.9
13	4.94	10.99	0.18	20.94	3.69	0.09	58.88
14	4.01	9.79	0.18	21.28	3.89	0.1	60.55
Average	**4.19**	**9.99**	**0.17**	**21.20**	**3.81**	**0.10**	**60.31**
Experimental Ks	***0.62***	***0.67***	***1.00***	***1.05***	***1.02***	***1.10***	***1.06***
Computational Ks	***0.42***	***1.18***	***0.40***	***1.03***	***0.99***	***0.94***	***1.01***

The experimentally determined Ks coefficients demonstrate that the elements Nb and Mo have a strong tendency to segregate in the intercellular area even in the case of very rapid cooling as it occurs when the material is additive manufactured, demonstrating the material anisotropy.

The analysis of the partition coefficients indicates that the elements Cr, Co, and Ni present a value slightly higher than one, demonstrating a more pronounced tendency of segregation in the center of the cells, while Ti and Fe can be considered neutral, having coefficients very close to unity.

Comparing the experimentally determined Ks coefficients to those predicted by Pandat^{TM}, the software's limitation was observed; it predicts correctly the segregation of Nb, Cr, Fe, Co, and Ni, but it doesn't predict the proper segregation of Mo and Ti. This is justified by the proportions in which these elements are found in the superalloy IN 625 (high Mo content, low Ti content).

Thermodynamic calculations performed to predict the fraction of phases developed, by using the chemical composition of the material intended for additive manufacturing, show that under equilibrium conditions (favorable conditions such as those of casting, where a reduced solidification rate is registered), in IN 625 can develop several phases. First of all, the main phase γ develops, which is found in a proportion of 100% up to about 1120 ° C, then precipitating the M$_6$C primary carbides.

At lower temperatures (approximately 960°C), the phase fraction γ is reduced, solid-state transformations take place, and phase δ precipitates. Besides, the σ phase and topologically compact compounds, such as Laves (noted by P_phase in the diagram in Figure 3.27), can precipitate.

Also, a reduction in temperature (about 800°C) can lead to the transformation of M$_6$C primary carbides to M$_{23}$C$_6$ type carbides. γ phase, carbides, and topologically compact phases (Laves) have been identified by other authors in the case conventionally manufactured superalloy IN 625 [247, 251, 252].

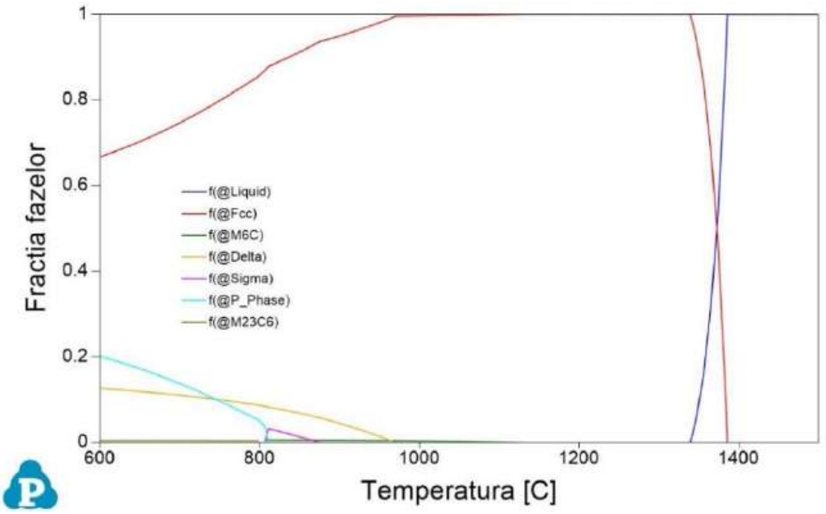

Figure 3.27. Prediction of phase fraction evolution in conventional manufactured IN 625

The solidification conditions experienced in case of the additive manufactured IN 625 are different, the solidification range is very short, and the material melts and solidifies very fast. For this reason, the unconventional manufactured material does not show solid-state transformations. Except for the γ phase, the M$_6$C primary carbides can precipitate directly from the liquid, but in very small ratios (less than 1%). Therefore, the phase fraction in the additive manufactured IN 625 material is shown in Figure 3.28.

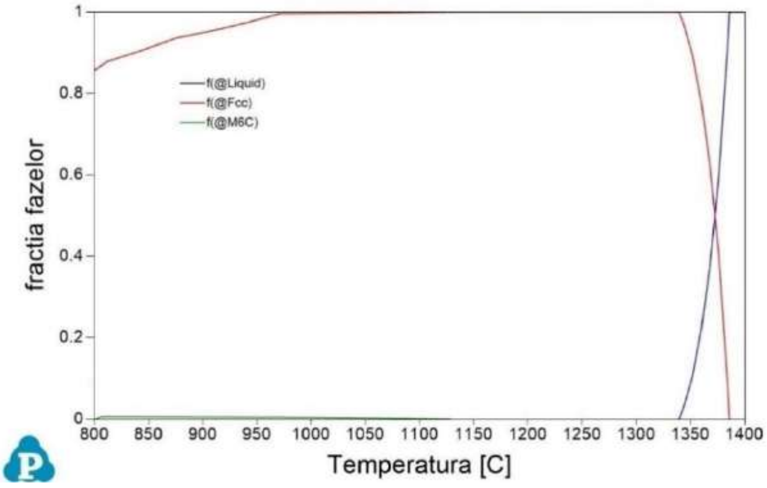

Figure 3.28. Phase fraction evolution in as-built additive manufactured IN 625

Nevertheless, following the application of heat treatments (stress relieving at 875 °C and solution treating at 1000°C), the precipitation of the δ phase is possible. Operation at high temperatures of the material can lead to the transformation of M_6C primary carbides into $M_{23}C_6$ complex carbides. Based on microscopic analysis different morphologies in the as-built IN 625 were observed, which led to the assumption that different phases developed during the solidification process.

Although the microstructure of the as-built material has different morphologies, after solidification, by EDS it was observed that a single phase was formed - the solid solution γ. Morphological differences are caused by the parameters used for the manufacturing process. X-ray diffraction analysis was also performed to confirm this partial conclusion.

The diffractometric analysis showed that the main phase developed is the γ phase that crystallizes in the FCC system with a network parameter a = 3,601 Å, and the secondary phases proportion recorded for the additive manufactured material in the as-built state was less than 1%.

The experimental results obtained from the X-ray diffraction are in a good agreement with the result obtained by thermodynamic calculations performed with PandatTM software. Based on all researches it was concluded that the SLM manufactured IN 625 is characterized by a strong microstructural anisotropy in the as-built state.

3.3. SLM process parameters' influence on the properties of IN 625

The experimental research on the SLM process parameters' influence on the properties of the IN 625 superalloy was performed using an iterative method that involves manufacturing specimens during several manufacturing cycles, and afterward, they were analyzed.

3.3.1. Iteration no. I – parameters' influence on the densification degree

The experimental research started using the optimum process parameters suggested by the equipment manufacturer, DMG MORI, for the material in question. The first batch of 15x10x10mm prismatic specimens was manufactured. The specimens were manufactured using a 90° scanning strategy with a change in the scanning direction by 90° after each layer. Representative images with prismatic specimens during the manufacturing process and after the SLM process are shown in Figure 3.34.

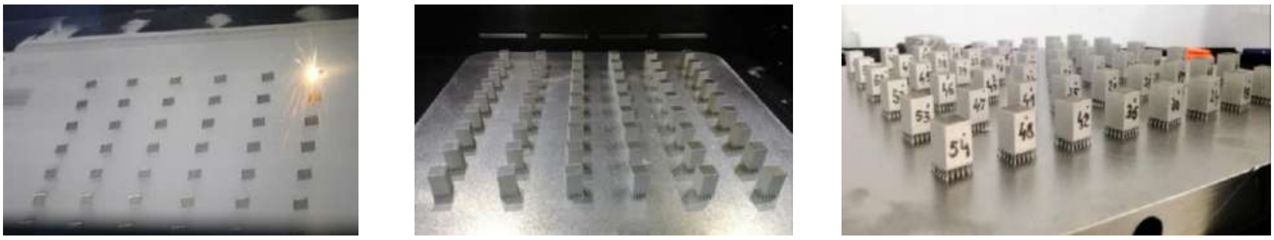

(a) (b) (c)

Figure 3.34. Representative images with the specimens manufactured during the first iteration: a) image during the manufacturing process; b, c) additive manufactured IN 625 specimens

After finishing the SLM process, the specimens were mechanically detached from the building plate, the support material being also mechanically removed (by grinding on abrasive paper). The density of specimens manufactured during Iteration no. 1 was in the range of 8430– 8450 Kg/m^3, which represents relative densities of 99.29% - 99.53%. Although there were differences between the specimens' density, the difference between them is smaller than the repeatability range r = 0.025 g/cm^3 accepted in the SR EN ISO 3369: 2010 standard [236]. Experimental research on the densification level of additive manufactured IN 625 material was performed by Gao et. al. [254] and Terris et. al. [255], obtaining different values of relative density in the range of 95.5 - 99.8%.

3.3.2. Iteration no. II – VED influence on the densification level

In this case, the experiments were performed based on the idea supported by several authors that there is a connection between the values of the volumetric energy density (VED) transmitted to the metal powder and the density of the additive manufactured material. Therefore, nine different values of the VED were defined based on a simplified model (a simplified matrix with three parameters - laser power, scanning speed, hatch distance on three levels).

The specimens were placed in the form of six groups composed of nine prismatic specimens, the specimens being manufactured using the specific parameters for each case. Each specimen corresponding to the same VED value was positioned identically for each group (Figure 3.36), and all groups were placed at the top of the building plate. A 90° scan strategy was applied for this iteration with the change in the scan direction by 90°.

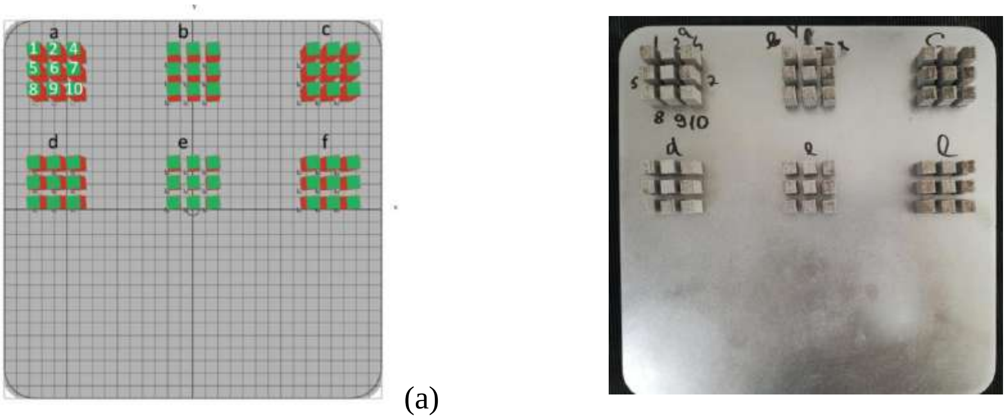

(a) (b)

Figure 3.36. Specimens' placement for Iteration no. 2: a) RDesigner image; b) specimen's placement on the building plate

It was found that the use of a 39 J/mm^3 VED value ensures the lowest results, the lowest density values were recorded in the case of group A (the relative densification level was even below 99%). The other VED values ensure the achievement of relative densification levels higher than 99% and within the limits of the repeatability interval imposed by the standard.

For this matrix, a microstructural analysis with finite elements was performed using the ANSYS Additive Suite program, the Additive Science module (Microstructure), R1 / 2020 edition. This program is based on the cellular automaton finite element method and can provide meaningful information on how the microstructure of an additive manufactured material develops.

The results of the microstructural simulations showed that the material's microstructure is textured, and it is strongly influenced by VED. It was observed that both the size of the equiaxed grains and columnar grains increases as the VED value increases (Figure 3.38.).

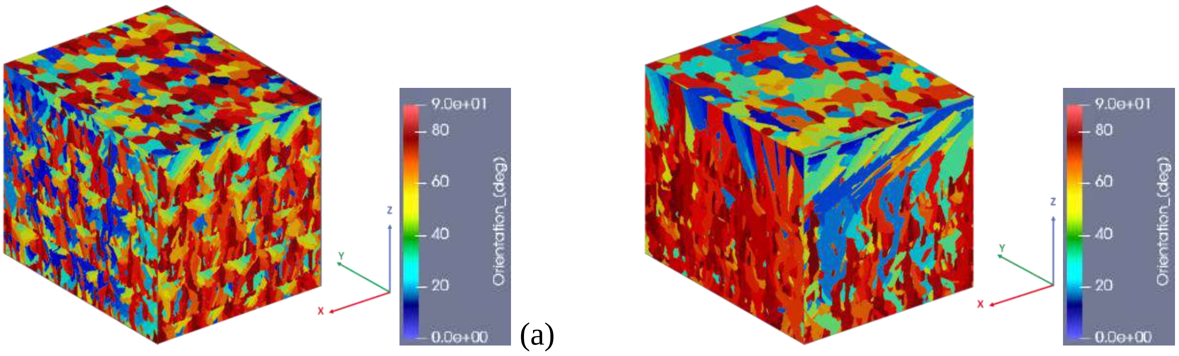

(a) (b)

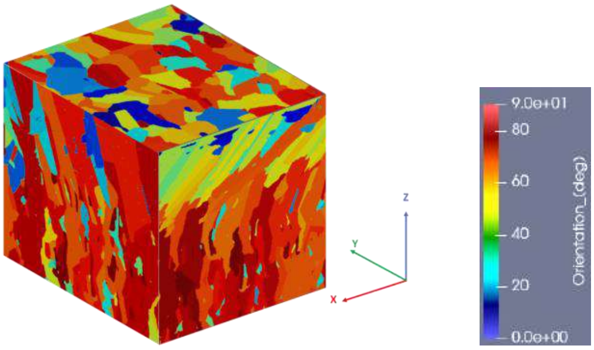

(c)

Figure 3.38. Representative images with the textured microstructure of the additive manufactured material using three values of the volumetric energy density: a) 39 J/mm^3; b) 69 J/mm^3; c) 97 J/mm^3

Using the values of the cooling rate determined by computational methods and the values of the primary dendrite arm spacing (λ_1) experimentally determined, the evolution of this morphological parameter was analyzed. In the scientific literature is mentioned that λ_1 may have different values depending on the cooling rate, for example in the case of large castings where the cooling rate is in the range of 10^{-4} - 10^{-2} K/s, λ_1 = 200 - 5000 μm, while in the case of laser melting/electron beam melting where the cooling rate is in the range of 10^3 - 10^9, λ^1 = 0.5 - 5 μm [257].

It was found that the value of λ_1 depends on the volumetric energy density, and representative SEM images with the dendritic structure identified for the additive manufactured IN 625 material, using different VED values are shown in Figure 3.40.

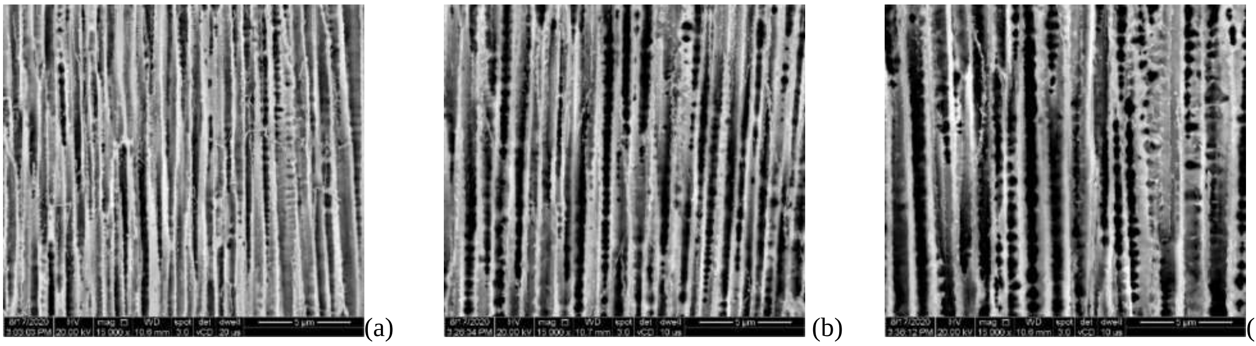

(a) (b) (c)

Figure 3.40. Representative SEM images with the dendritic microstructure identified in the additive manufactured IN 625 material: a) VED = 39 J/mm^3; b) VED = 69 J/mm^3; c) VED = 97 J/mm^3

3.3.3. Iteration no. III – VED and scanning strategy influence on the material's properties

Starting from the results recorded in the case of Iteration no. 2, the same simplified matrix was used to manufacture a new specimen batch, this time applying a 67 ° scanning strategy.

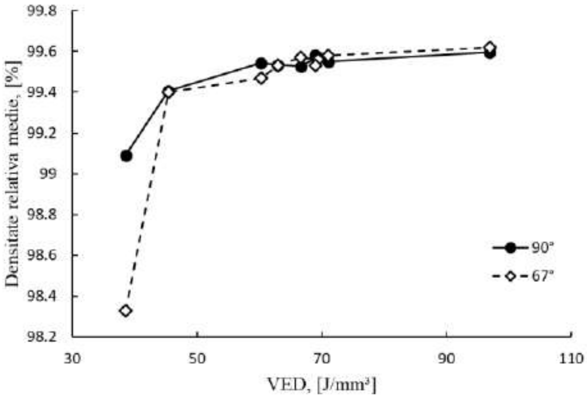

Figure 3.42. Comparative graphic representation of medium relative densities determined for the Iteration no. 2 and 3 (90° and 67° scanning strategies) as a function of volumetric energy density

The best relative density values were obtained for the highest VED value - 97 J / mm3 (relative density of 99.60% for the 90° scanning strategy, the relative density of 99.62% for the 67° scanning strategy). The lowest relative density values were recorded at the lowest VED value - 39 J / mm3 (relative density of 99.09% for the 90° scanning strategy, the relative density of 98.33% for the 67° scanning strategy).

Of the two scanning strategies, the 67° scanning strategy provides both the lowest relative density value and the highest relative density value. The low level of densification recorded at low VED values is a result of the material presented lack of fusion defect, LOF being identified in the surface of the specimens. The proportion of these defects decreases as the VED value increases (Figure 3.43).

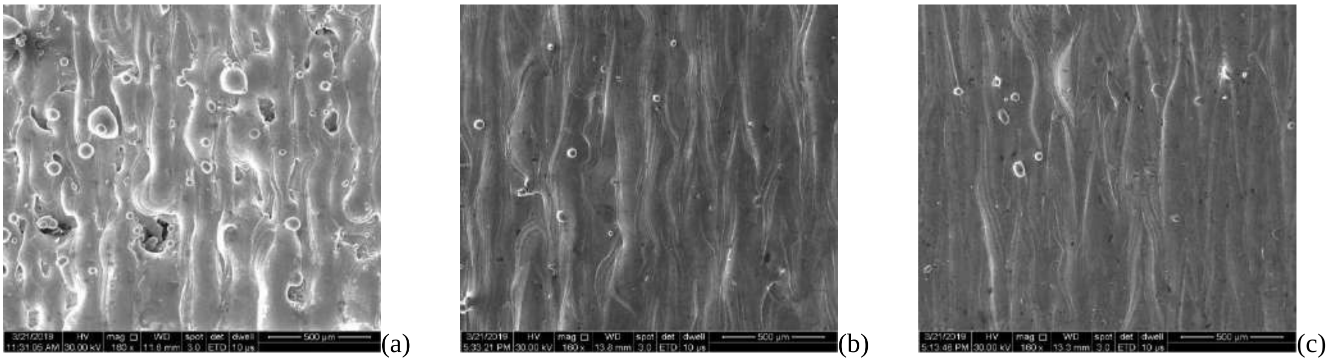

Figure 3.43. VED influence on the LOF defects: a) VED – 39 J/mm^3; b) VED – 69 J/mm^3; c) VED – 97 J/mm^3

In addition to LOF defects, certain combinations of parameters led to an instability of the metal melt, which causes splashes to be ejected from the melt pool during the scanning process. These splashes can in some cases drag along powder particles from the powder bed; they attach to the side surfaces of the specimens and solidify in this area. These phenomena lead to an increase in the roughness of the material (Figure 3.44).

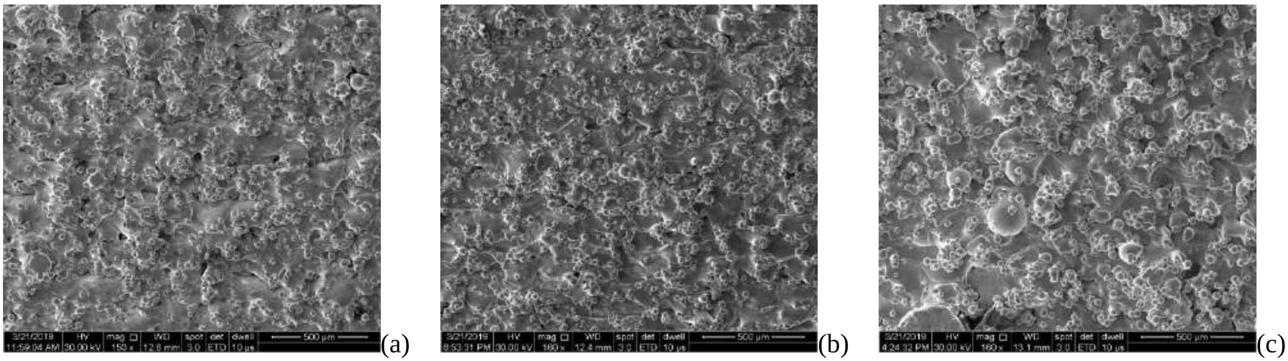

Figure 3.44. VED influence on the balling effect: a) VED – 39 J/mm^3; b) VED – 67 J/mm^3; c) VED – 97 J/mm^3

It was found that the surface roughness increases simultaneously with the increase of the VED value. High VED values ensure the highest surface roughness. Analyzing the results according to the applied scanning strategy, it was determined that the 67° scanning strategy results in higher roughness compared to the roughness determined in the case of the batch manufactured using the 90° scanning strategy (Figure 3.45).

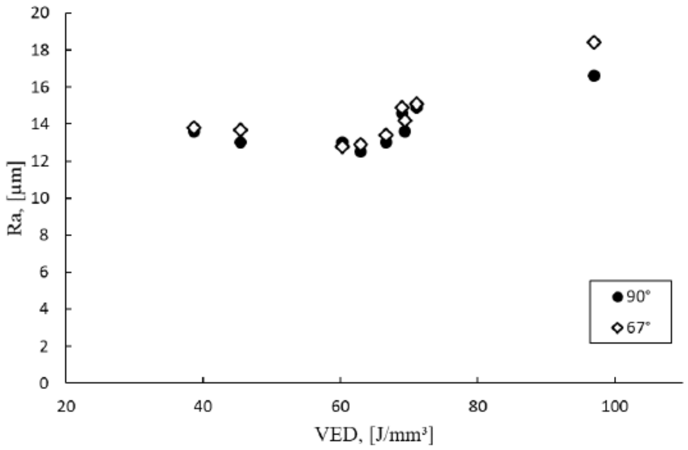

Figure 3.45. Lateral surfaces roughness evolution as a function of volumetric energy density

Given the fact that the batch manufactured applying the 67° scanning strategy has a higher level of surface defects additional analyses were performed to identify other types of defects that occur in the case of these specimens. Therefore, determinations of the porosity level and dimensional analysis were performed.

The results obtained in the case of porosity demonstrate that VED has a significant influence on the porosity level (Figure 3.46). As the VED value increases, the pore degree decreases. Using low VED values there is a sudden increase in porosity mainly due to LOF defects.

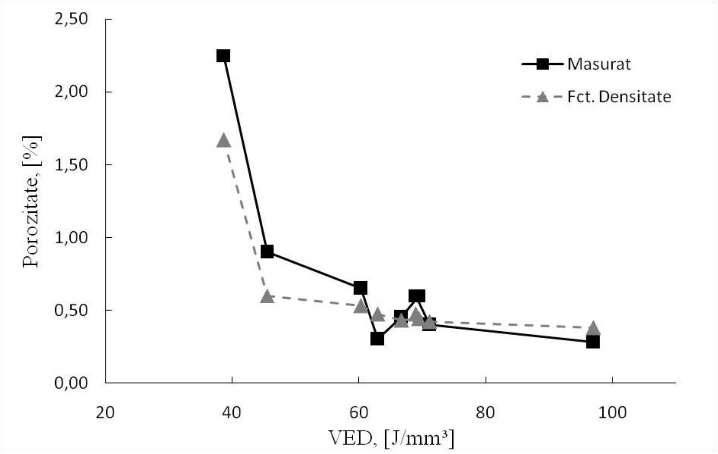

Figure 3.46. Roughness presented as a function of the volumetric energy density

Except for surface defects, such as balling and LOF, it was found that in the XOY plane, the specimens were deformed at the edges and corners, so the top surface of all specimens in this batch was 3D scanned to determine the influence of process parameters on the degree of deformation. As the value of the volumetric energy density increases, so does the width of the distorted area near the edges of the specimens. The variation of the distorted width is shown graphically in Figure 3.50. In addition to the distorted area near the edges, there was also an increase in the height of the corners and edges (Figure 3.51), also dependent on the VED value.

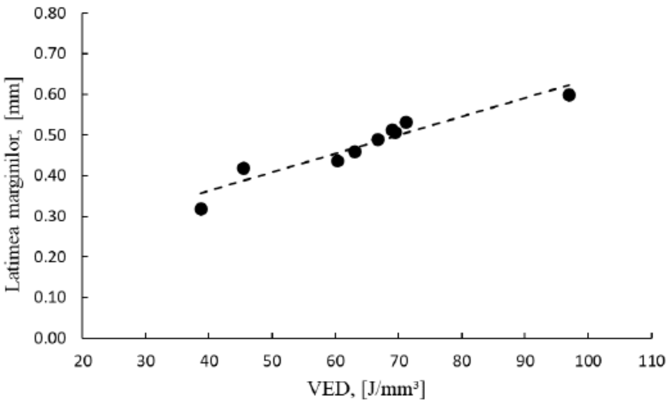

Figure 3.50. Changes in edge width as a function of VED

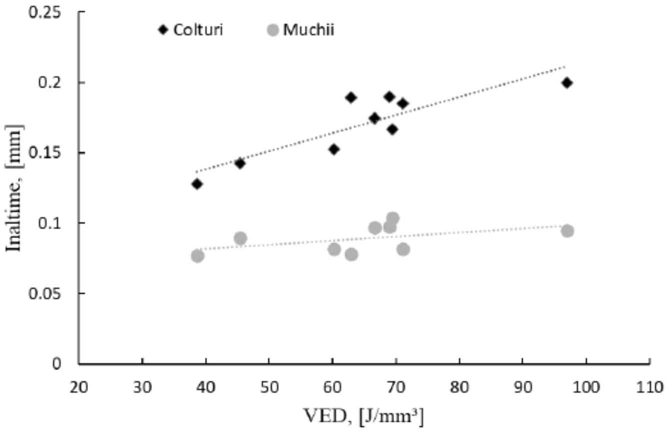

Figure 3.51. Changes in corner and edge heights as a function of VED

By using high VED values (high laser power, low scanning speed) a large amount of heat is produced, the melt pool becomes unstable, and it is pushed to the side of the specimens. As the energy increases, the level of surface deformation increases. To ensure a balance between all the phenomena that occur and to maintain the stability of the melt pool, laser powers in the range of 250 - 320 W and scanning speeds of 0.6-0.8 m / s should be used.

Similar to the results registered in the case of finite element microstructural simulations performed for the batch of specimens manufactured by using a 90° scanning strategy, it was found that in the case of applying a 67° scanning strategy, the microstructure is textured and strongly influenced by the volumetric energy density value. By computational methods, it has been found that both the size of the equiaxed grains and the size of the columnar grains increase as the value of the volumetric energy density increases (Figures 3.52).

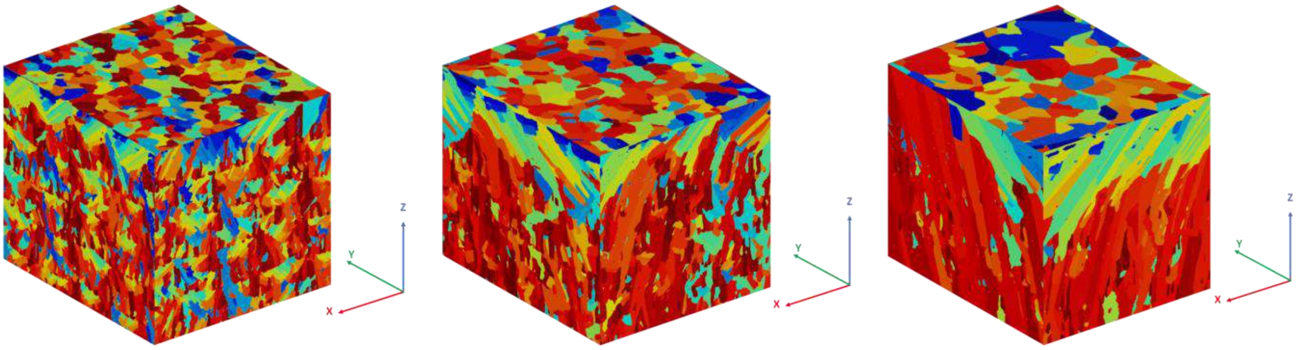

(a) (b) (c)

Figure 3.52. Representative images with the textured microstructure of the additive manufactured material using the 67° scanning strategy and three different VED values: a) 39 J/mm^3; b) 69 J/mm^3; c) 97 J/mm^3

The 67° scanning strategy ensures lower λ_1 values compared to the 90° scanning strategy. It was found that λ_1 respects the relations $\lambda_1 = 153.88 \cdot (R)^{0.388}$ (for the material manufactured applying the 90 ° scanning strategy) and $\lambda_1 = 151.98 \cdot (R)^{0.385}$ (for the material manufactured applying the 67 ° scanning strategy). The obtained relations are close to the theoretical relation of $\lambda_1 = \text{ct.}\ (R)^{(0.3 \pm 0.03)}$, but also to the relation obtained by Matache et.al. [216] $\lambda_1 = 151.98 \cdot (R)^{0.34}$ for a Ni-based superalloy manufactured by conventional methods.

3.3.4. Investigations on microstructural anisotropy and the influence on tensile mechanical property

Microstructural anisotropy was highlighted both experimentally by light microscopy analysis and by computational methods (Figure 3.57). Given the limitations of the software, simulations were performed in the case of specimens manufactured parallel to the OZ axis, applying process parameters: hatch distance of 0.11 µm, the layer thickness of 40 µm, laser power of 250 W, scanning speed of 750 mm / s, the temperature of the building plate of 80°C, laser focus 80 µm and the two scanning strategies: at 90°, 67° with changing the scanning direction by 90°.

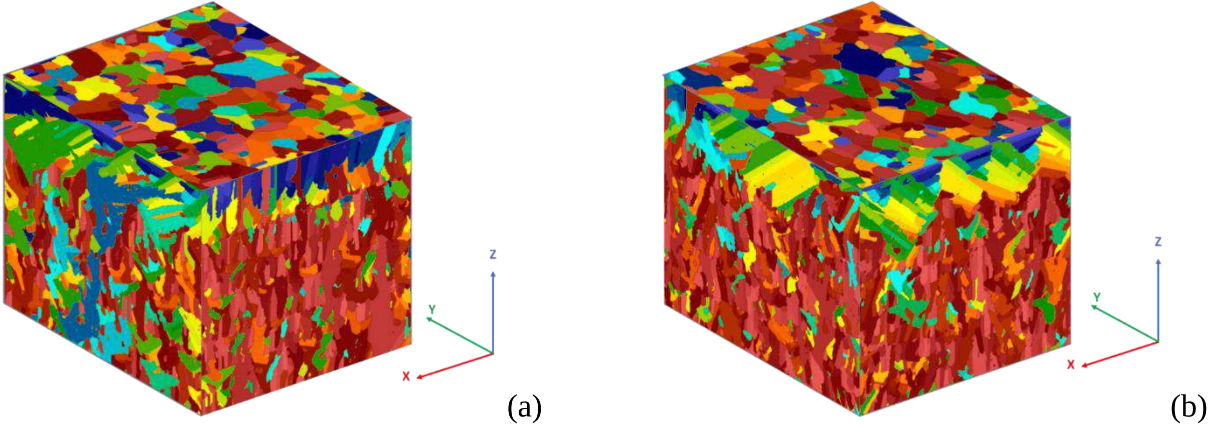

(a) (b)

Figure 3.57. Additive manufactured material's microstructure developed by appling a 90° scanning strategy (a), respective 67° scanning strategy (b)

From the images presented in Figure 3.57 it can be seen that applying a 90° scanning strategy, columnar grains develop in the XOZ and YOZ planes, they are growing on multiple layers, while in the XOY plane equiaxed grains were obtained. It can be noticed that the scanning strategy affects the way the as-built microstructure develops. These morphological differences are caused by the differences in the thermal gradient and cooling rate. The software predicts a cooling rate of 470.161 K / s and a thermal gradient of 4.409.697 K / m when the 90 ° scanning strategy is applied, while a cooling rate of 505.644 K / s and a thermal gradient of 5.392.682 K / m are registered when the 67 ° scanning strategy is applied.

The experimental morphological analysis of the grains in the as-built state is difficult, so it was preceded to the microscopic analysis of the additive manufactured material after heat treatment (stress relieving 870°C / 1h, air cooling, solutionizing heat treatment 1000 °C/1h - oil quenching). By applying these heat treatments it is aimed to reduce the material's high internal stress that was induced during the manufacturing process and to improve the material's workability (IN 625 manufactured additive has a low ductility in the as-built state and is difficult to machine).

After the heat treatment was applied, the material's recrystallization takes place and the similarities between the experimental and computational results are observed (Figure 3.59). Columnar grains that grew on multiple layers were identified for both scanning strategies (view in the YOZ and XOZ planes) and equiaxed grains developed on the XOY plane for specimens manufactured using both scanning strategies.

After heat treatment, besides microstructure recrystallization, packaging defects (annealing twins and growth twins) were also observed. Such defects have been identified by other researchers both in the case of the material manufactured by conventional and additive methods [97, 260, 261].

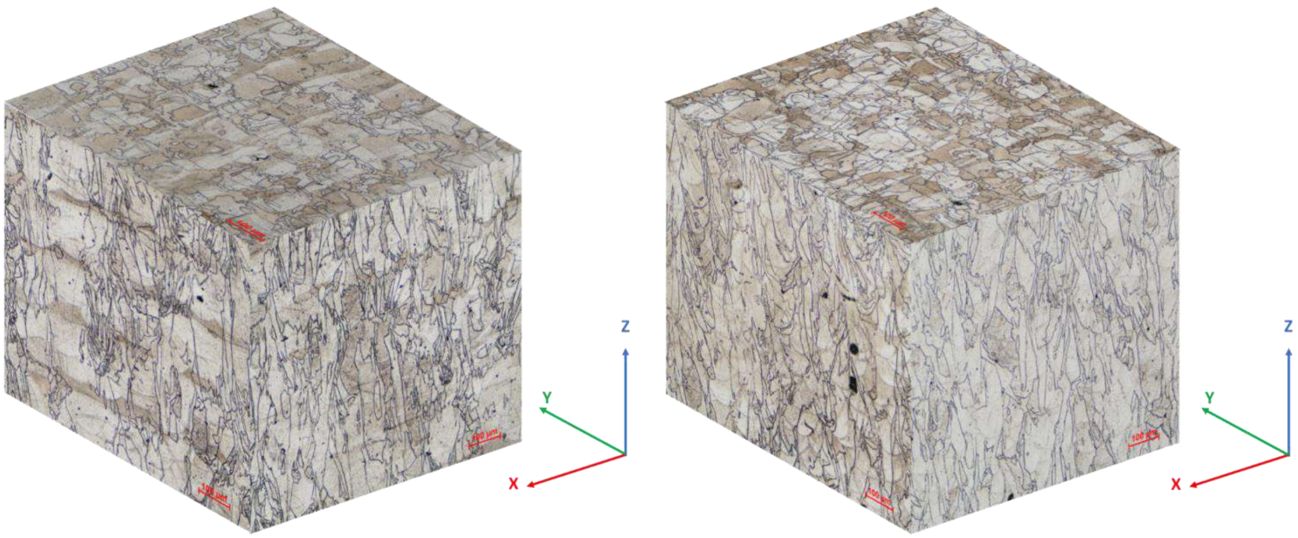

(a) (b)

Figure 3.59. Images with the additive manufactured IN 625 microstructure after heat treatment, obtained using the scanning strategy at: a) 90°; b) 67°

The microstructural anisotropy is maintained even after heat treatment, and according to the literature, this anisotropy affects the mechanical properties. Thus, batches of specimens were designed for tensile testing, specimens build parallel to the OX, OY, and OZ axes, by applying the two scanning strategies at 90 ° and 67 ° with the scanning direction change by 90 °.

Based on the results of the tensile tests, it was found that all the average values obtained for Rm, Rp$_{0,2}$, Z, and A$_5$, regardless of the scanning strategy applied or the orientation at which the specimens were manufactured, are higher than the minimum values accepted by the active standards for conventionally manufactured IN 625 (Rm = 485 MPa, Rp$_{0,2}$ = 275 MPa, Z and A$_5$ 30% according to ASTM B443 [239]) as well as for the material manufactured by powder bed methods (Rm = 758 MPa, Rp$_{0,2}$ = 379 MPa, Z and A$_5$ 30% according to ASTM F3056 [98]). The comparative analysis of the results according to the orientation on the building plate is presented in Figure 3.63.

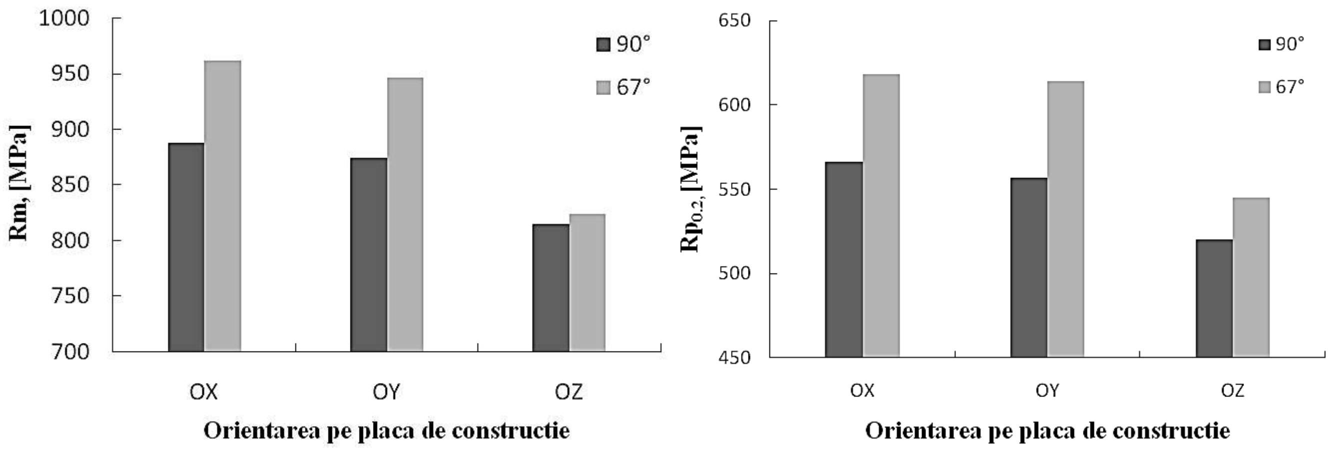

(a) (b)

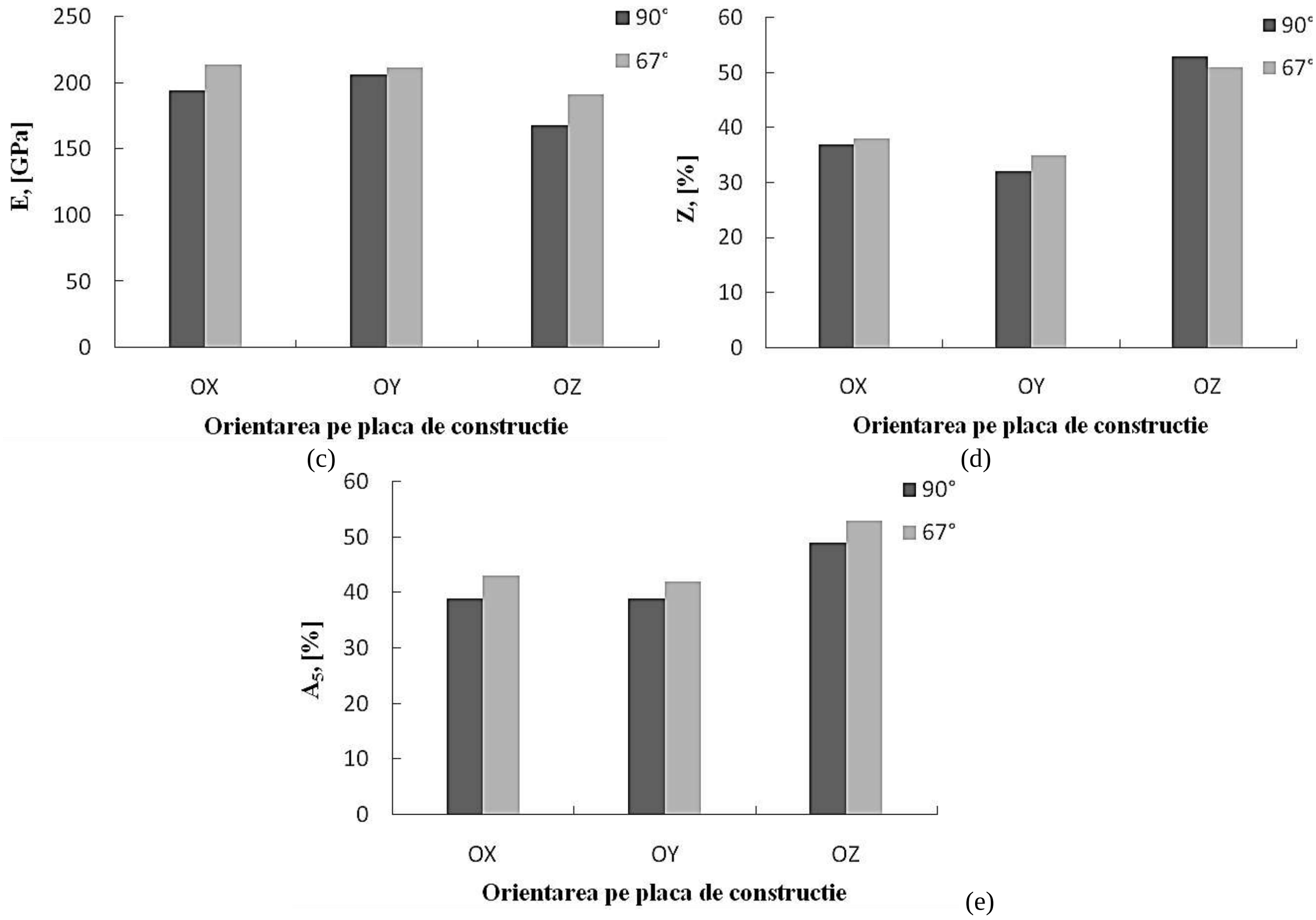

(c) (d)

(e)

Figure 3.63. Tensile test results as a function of the building orientation: a) Rm; b) $Rp_{0,2}$; c) E; d) Z; e) A_5

Studying the charts from Figure 3.63, it was found that the building orientation has a significant influence on the tensile strength of SLM manufactured IN 625. Specimens manufactured in a vertical position (parallel to OZ axis) have the lowest tensile performance, while specimens manufactured in the XOY plane have higher tensile strengths than those manufactured in a vertical position. No significant differences were observed between the specimens manufactured parallel to the OX and OY axis. The same trend was registered in the case of the $Rp_{0,2}$ and E values. The specimens manufactured in vertical position show the highest values of area reduction and elongation. The comparative analysis of the results is presented graphically in Figure 3.64.

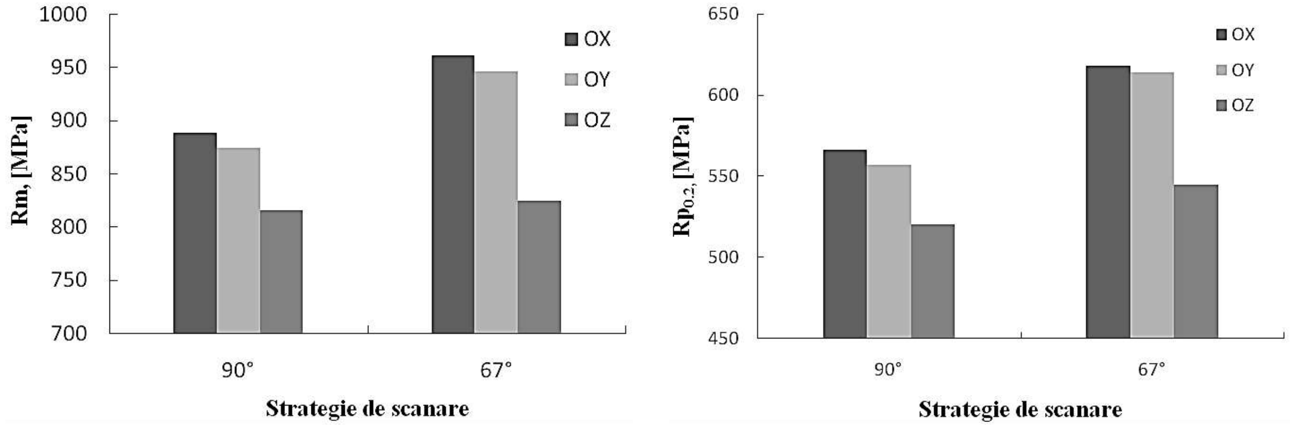

(a) (b)

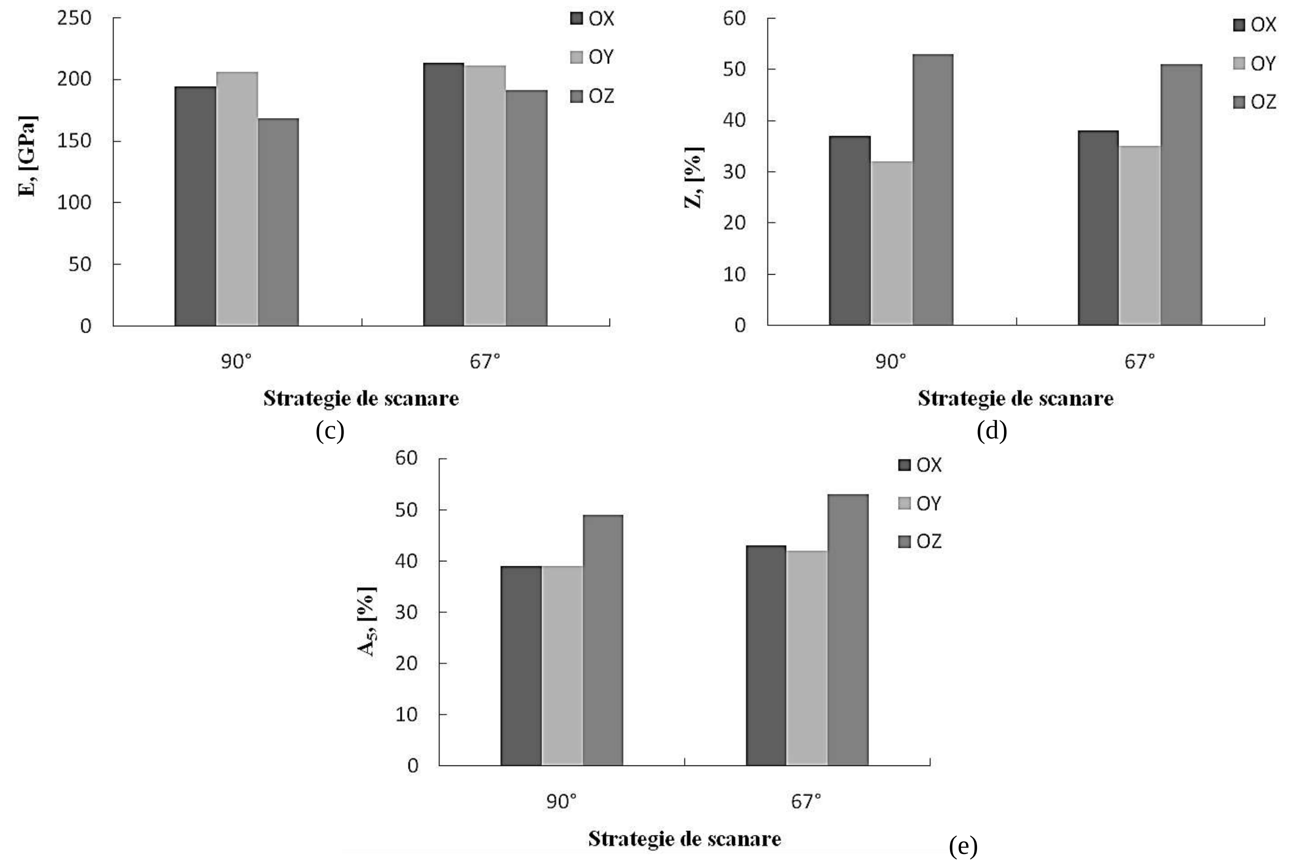

(c) (d) (e)

Figure 3.64. Tensile test results as a function of the applied scanning strategy: a) Rm; b) $Rp_{0,2}$; c) E; d) Z; e) A_5

The scanning strategy influences the mechanical characteristics, the highest values of tensile strength, and yield strength are recorded in the case of manufactured specimens applying a 67° scanning strategy. The 90° scanning strategy ensures the lowest room temperature tensile performances, regardless of the orientation on the specimen building orientation.

The values recorded indicate a highly evident anisotropy level of the additive manufactured material parallel to the OX or OY axes relative to the material manufactured in the vertical position. This anisotropic character is caused by the applied tensile stress direction relative to the material’s grains growth direction (Figure 3.65).

In the case of specimens manufactured in the OZ axis, the stress is applied parallel to the growth direction of columnar grains, while in the case of specimens manufactured on the OX and OY axis, the tensile stress is applied perpendicular to the growth direction of columnar grains.

The SLM manufactured IN 625 superalloy was fractured in a complex way, which is a combination of ductile and brittle fracture. Matt fibrous areas specific to ductile rupture and bright crystalline areas specific to brittle fracture have been identified. These results are in good agreement with those obtained by other authors for the same material in a heat-treated state [262].

3.4 High temperature exposure influence on the oxidation behavior of SLM melted manufactured IN 625 superalloy

The IN 625 material is commonly used for the manufacturing of gas turbine components that currently operate at temperatures up to 900 ° C and for short periods at higher temperatures in oxidizing environments. Based on these facts, it is necessary to study the behavior of the additive manufactured material following exposure to high temperatures in an oxidizing environment and to carry out a comparative study between the behavior of the conventional manufactured material and advanced method manufactured material. Research on the influence of high-temperature exposure on the oxidation behavior of SLM manufactured IN 625 was performed at two temperature values (900 ° C, 1050 ° C) during 96 h.

The experiments carried out to determine the influence of prolonged elevated temperature exposure to the additive manufactured IN 625 consisted of:
- test specimens manufacturing;
- conducting experimental research on the oxidation process kinetics;
- conducting experimental research to characterize the oxide scale developed;
- conducting experimental research on the influence of high-temperature exposure on tensile strength.

3.4.1 Experimental research on the oxidation process kinetics

The mass gain analysis of specimens exposed to high temperatures showed that the oxidation process at both temperatures follows a parabolic law. IN 625 oxidized at 1050 ° C shows a much higher mass gain compared to 900°C oxidized material. Although the oxidized material at 900°C follows a parabolic law, at exposure times longer than 24 h, the process appears to be more linear. This observation is consistent with the results obtained by other researchers in the case of Ni-based superalloys exposed to various oxidation processes, which comply with a sub-parabolic law at temperatures up to 900°C and a parabolic law at higher temperatures [147, 264-266].

3.4.2. Characterization of the oxide scale developed

The EDS analysis of specimens' surfaces revealed that after a total of 96 h of high-temperature exposure, the process led to the formation of mainly chromium oxide scales. Based on the analysis realized on oxidized specimens at 900°C besides O and Cr small traces of Mo, Nb, and Fe were identified, while only small traces of Nb and Fe were identified in the case of oxidized specimens at 1050°C (Figure 3.72).

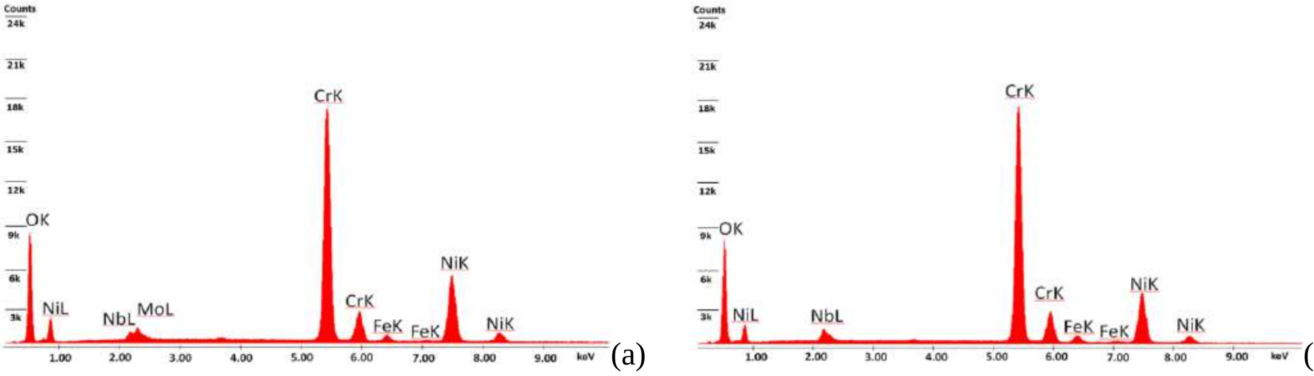

(a) (b)

Figure 3.73. EDS spectra on the top surfaces of oxidized specimens at 900 °C (a) and 1050 °C (b) [263]

In order to determine which chemical elements, react with oxygen during its diffusion in the baseline material and whether a reduction in the overall metal at the specimen's surface is registered, an EDS analysis was performed in four microareas (three in the oxide scale and one in the base material under the interface with the oxide layer) in the specimen's cross-section.

The quantitative chemical analysis of the specimen surface shows that after the first 24 h of the oxidation process at 900°C, the oxide scale contains, besides Cr, different amounts of other oxide forming alloying elements, such as Ni, Nb, Mo, and Fe. Thus, it can be concluded that the oxide scale consists of chromium oxide and other spinels or oxides containing these elements.

Different chemical compositions were determined for the specimens oxidized at 900°C and 1050°C. At 1050°C, the specimens' surface is practically free of significant amounts Mo and Fe, with

small amounts of Nb and Ni being present apart of Cr. The high temperature oxidation process ensures the formation of mainly chromium oxide starting from the incipient maintenance cycles.
In order to identify the alloying elements reparation as oxides or other phases, both oxidized specimens were analyzed by X-ray diffraction.

The isothermal oxidation at 900 °C and 1050 °C for small periods of time promotes the precipitation of δ phase ($(Mo, Nb) Ni_3$) (phase predicted also by thermodynamic calculations), an Ni-rich intermetallic (MoNi4), and complex carbides ($(Cr, Fe, Mo, etc.)_{23}C_6$). The oxide scale formed within 24 h at 900°C consists mainly of Cr_2O_3 followed by the spinel $(Ni,Fe)Cr_2O_4$, while at 1050°C it consists mainly in spinel $(Ni, Fe)Cr_2O_4$, followed by Cr_2O_3. Moreover, in case of oxidation at higher temperature (1050 °C) another oxide characterized by a rutile-like structure ($(((Cr^{+3}(Nb, Ta)^{+5})_{(1-x)/2},(Ti^{+4})_{x})O^{-2}_{2})$ was identified.

Secondary phases as δ, Ni-rich intermetallic and complex carbides were identified by other authors [256,260, 270,271]. After prolonged temperature exposure at 900 °C only the complex carbides dissolves, the γ and δ phases were still present along with the MoNi4 intermetallic while the prolonged higher temperature exposure led to the dissolution of the δ phase, MoNi4 intermetallic, and carbides.
Optical microscopy analysis revealed microstructural changes caused by the material's high temperature exposure (Figures 3.76, 3.77).

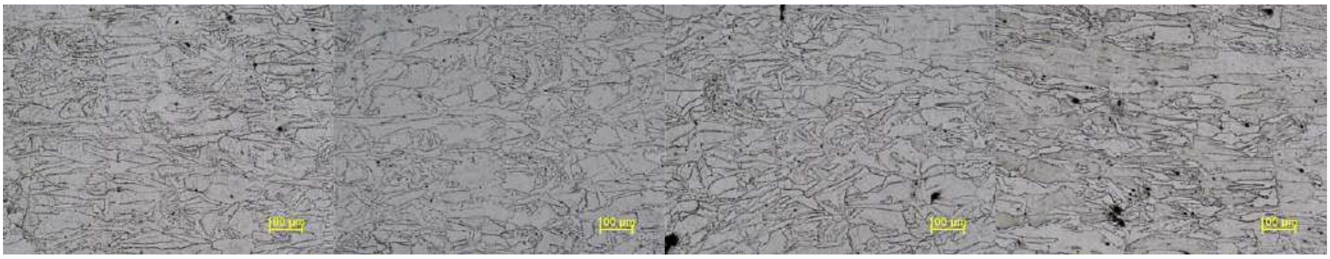

(a) 24h (b) 48 h (c) 72 h (d) 96 h

Figure 3.76. Optical microscopy images showing the SLM manufactured IN 625 microstructure after 900°C (XOZ plane)

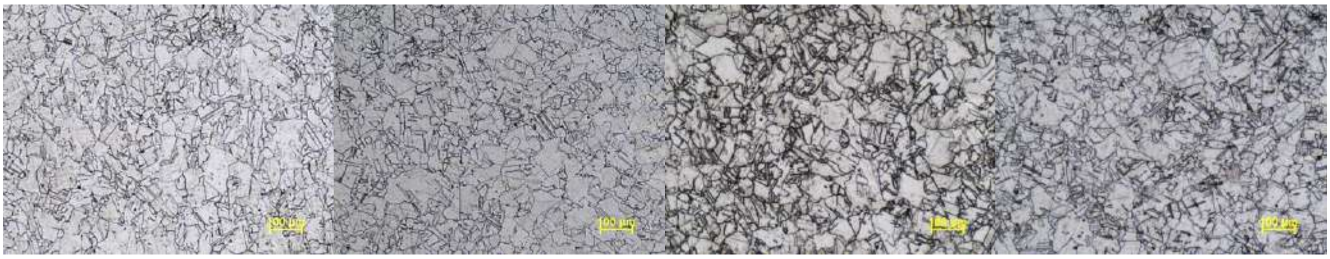

(a) 24h (b) 48 h (c) 72 h (d) 96 h

Figura 3.77. Optical microscopy images showing the SLM manufactured IN 625 microstructure after 1050°C (XOZ plane)

Exposure to 900°C led to a material's recrystallization, and the formation of a structure similar to the microstructure observed when applying the pre-established heat treatment for additively manufactured IN 625. The microstructure does not change during the 96 h of exposure at 900°C because the temperature is within the heat treatment temperature range of the material. Microscopic analysis performed in the same plane in the case of 1050°C oxidized specimens shows recrystallization of the material, the columnar grains transformed into equiaxed grains. The morphology of the equiaxed grains formed in the first stages of isothermal oxidation at 1050°C does not change after increasing the duration of exposure, the only difference being the number of annealing twins, prolonged exposure led to an increase of twins.

The morphologic evolution of the oxide scale was assessed based on SEM analysis and different morphologies were observed for the oxides developed at the two high temperatures. The oxide scale formed at 900 °C presents a more angular morphology compared with the rounder morphology observed in the case of the oxide scale formed at 1050 °C. Moreover, the oxide scale formed during oxidation at 1050 °C looks more porous than the oxide scale formed at lower temperatures, which is more compact.

The evolution of oxide scale during the exposure time at the high temperature was assessed by thickness measurements. A parabolic evolution of the oxide scale thickness as a function of time was registered in both types of oxidation processes. A significant difference between the oxide scale's thicknesses for the two temperatures was registered. The thickness of the oxide scale formed at 1050 °C is almost double when compared with the oxide scale formed at 900 °C. The oxide scale thickness increases fast during the first 24 h of exposure, then the increase is more moderate between 24–96 h at both temperatures. During the exposure between 24–96 h, the oxide scale thickness increases at 900 °C is lower than at 1050 °C.

As it was noticed in the case of mass gain and oxide thickness evolution analysis, oxidation for longer periods over 72 h at 1050 °C generates a decrease in the oxide's thickness, along with a reduction of the specimen's mass gain. This reduction of the scale thickness recorded after 72 h of exposure is caused by the oxide scale spallation. This was observed in case of specimens oxidized at 1050 °C, the oxide scale spallation was not observed in the case of specimens oxidized at 900 °C, the oxide scale formed in this case being denser and more even than the scale formed in the case of oxidized specimens at higher temperatures. A similar behavior was reported by N'dah et.al. [268] for 900°C oxidation of conventional manufactured IN 625 exposed for 50 h. Voids and cavities were observed in the porous scale formed at 1050 °C, consistent with the defects also found by other researchers in case of the IN 625 superalloy manufactured by conventional methods [268, 278]. After the 10th cycle a specimens' weight decrease was recorded, it being caused by oxide scale spallation. Oxide scale spallation and mass gain decrease were also noticed by other authors [265, 267, 277]. However, the oxygen diffusion continues, and an increase of the specimen's weight was recorded during the following oxidation cycles.

3.4.3 Experimental research regarding the high temperature exposure influence on the tensile strength

In as-built state, the additive manufactured material parallel to the OX axis has a value of Rm = 900 MPa, $Rp_{0.2}$ = 595 MPa, Z = 20%, A_5 = 27%. Comparing the results obtained in the case of as-built specimens manufactured parallel to the OX axis with those obtained for the heat-treated specimens, manufactured parallel to the OX axis, it was found that the tensile strength and the yield strength are not significantly affected by the heat treatment. Significant differences are observed in the case of elongation and area reduction, in the as-built state the alloy shows lower values compared to the values recorded after heat treatment, the heat treatment cycles increasing the ductility of the material.

Repeated exposure to 900°C does not significantly affect the tensile strength and yield strength of the SLM manufactured IN 625 superalloy. As the microstructure of the material does not change during the 96 h exposure at 900°C, no significant changes were recorded regarding the mechanical properties determined by the tensile test.

If no major changes were recorded after repeated exposure at 900°C, a different situation was recorded for the material exposed at higher temperatures. Exposure for 24 h at 1050°C led to a sudden reduction of Rm and $Rp_{0.2}$ by 10% (from 900 MPa to 807 MPa) and 39% (from 595 MPa to 362 MPa), respectively. Subsequently, the material does not register significant changes in the values Rm and $Rp_{0,2}$.

The 24 h exposure at 1050°C ensures an increase in Z and A_5 (an increase of 60% was recorded for Z - from 20% to 33%, respectively an increase of 63% in the case of A_5 - from 27% to 44%), and then no significant changes occurred. The reduction of tensile strength and yield strength after exposure for 24 hours at 1050 ° C is the result of changes in grain morphology, the high strength of the additive manufactured material parallel to the OX axis being ensured by the tensile load perpendicular to the columnar grains growth direction, and the high-temperature exposure alters the grain morphology.

CONCLUSIONS

Within this thesis, theoretical and experimental researches were carried out regarding the prediction and optimization of the characteristics of the Ni-based superalloy, IN 625, manufactured by the advanced additive manufacturing technology from metallic powder, selective laser melting method.

►The experimental researches performed regarding IN 625 powder's characteristics evolution in time, as a result of its recirculation, led to the conclusion that there are no significant changes in the physical and technological powder's characteristics. All results support the hypothesis that IN 625 powder intended for additive manufacturing may be used/reused during several manufacturing cycles. Sieving the powder between manufacturing cycles doesn't influence the characteristics of the products manufactured by this method.

► Thermodynamic calculations in multicomponent systems were realized using Pandat^{TM} software, based on the CALPHAD method. It was concluded that changing the compositional range of IN 625 main alloying elements – Nb, Mo, Cr - has a significant influence on the transformation temperatures and its phase ratio (even within the chemical limits accepted by the standard). The results obtained employing Pandat^{TM} for IN 625 manufactured by conventional methods were extrapolated to the additive manufactured material.

►Both computational and experimental methods demonstrated the tendency of the alloying elements to segregate preferentially, even in the case of very fast solidification of the additive manufactured material, and the proportion of phases resulting in raw printed material was predicted.

►By computational methods, the material's secondary phases that can precipitate following operation of additive manufactured IN 625 components at high temperatures or after material's high temperature exposure were predicted. This conclusion has been confirmed by experimental research realized to analyze the influence of high temperatures exposure on the additively manufactured material's behavior.

►Typical microstructural characteristics for additive manufactured materials were highlighted by using the ANSYS Additive Suite software and experimental methods. The microstructural anisotropy of SLM manufactured IN 625 with different process parameters was demonstrated.

►It was experimentally proven that SLM process parameters have a significant influence on the IN 625's characteristics. The volumetric energy density (VED) is a parameter that can be used to control/manage the material's characteristics as VED values have a significant influence on the material density level, primary dendrite arm spacing, internal and external defects.

►It was concluded that to obtain additive manufactured products by SLM with a maximum densification degree and minimum defects, are required laser powers within the range of 250-320 W and scanning speeds within the range of 0.6-0.8 m/s.

►It was established based on the experimental researches that SLM manufactured IN 625 has a higher tensile strength than its conventional manufactured counterpart. To obtain the IN 625 with the highest tensile strength the parts should be laid on the building plate in a position that allows a preferential development of the microstructure to a certain direction and the subsequent mechanical stress should occur perpendicular to the growth direction of the columnar grains.

►The results obtained from the research conducted on the determination of high-temperature exposure in an oxidizing environment on the additive manufactured IN 625 superalloy showed that there are significant differences between the behavior of the additive manufactured IN 625 as compared with the behavior of the same material manufactured by conventional methods.

The general conclusion regarding the application of computational methods for prediction and optimization of characteristics of Ni-based superalloys, manufactured by advanced methods such as additive manufacturing technology, is that current programs using such methods are not sufficiently advanced, but they can provide meaningful information on phase development and microstructure. Further experimental research must be done to adjust the existing software databases for additive manufactured materials and to develop new databases for several types of additive manufacturing alloys.

However, the advantages of computational methods are very obvious as they can greatly reduce both the characteristics optimization time of additive manufactured materials and material losses.

PERSONAL AND ORIGINAL CONTRIBUTIONS

For the development of the current state of the art in the field of additive manufactured Ni-based superalloys by SLM method and in the field of computational methods used for prediction and optimization of characteristics of additive manufactured materials, I've had the following personal contributions:

Ni-based superalloys manufactured additive by SLM method and computational methods for forecasting and optimizing the characteristics of additive manufactured materials, we had the following personal contributions:

1. I have conducted researches in the scientific literature that allowed me to identify the current state of the art in the field of additive manufacturing and computational methods used to predict and optimize the characteristics of metallic materials manufactured by advanced methods such as the SLM method. The research led to the elaboration of a work plan and a methodology that involved two well-known computational methods in the field of prediction and optimizing the structure of metallic materials manufactured by conventional methods and usual analysis methods that were applied to characterize additive manufactured IN 625 material.
2. Putting together thermodynamic calculations in multicomponent systems with the prediction of microstructure formation in additive manufactured materials by the cellular automaton finite element method and experimental research is an original approach used to achieve the thesis objectives, being a national novelty and a priority of the international scientific community.
3. The recycling of metal powders intended for additive manufacturing is an internationally debated topic, and it was also addressed during the Ph.D. thesis. An evaluation method was defined to determine the IN 625 powder characteristics evolution in time after recirculating it. The method integrates powder metallurgy specific methods used for powder characterization with software used for microscope image processing. The method was used to highlight the fact that additive manufacturing IN 625 powder can be used/reused during several manufacturing cycles without changing its characteristics.
4. Originally I have combined a statistical model (matrix 33) with the CALPHAD computational method, to determine the concentration of main alloying elements of IN 625 superalloy - Nb, Mo, Cr, influence on the transformation temperatures and the phase ratios. The results obtained for IN 625 manufactured by conventional methods were extrapolated to the additive manufacturing situation.
5. Based on the thermodynamic calculations performed, I have identified a limitation of the thermodynamic database of the Pandat^{TM} software (PanNi2020_TH) regarding the analysis of the segregation tendency of Mo, Ti alloying elements.
6. Originally, I have put together a simplified statistical model with the computational research based on the cellular automaton finite element method and the experimental research. These results highlighted the microstructural anisotropy of IN 625 material additive manufactured by the SLM method.
7. I have experimentally demonstrated that the volumetric energy density parameter – VED can be used to control/manage the characteristics of the additive manufactured IN 625 superalloy.
8. I have narrowed the range of the main additive manufactured process by selective laser melting – SLM in terms of laser power and scanning speed to the range of 250-320W, respectively 0.6-0.8 m/s. Different combinations of values can be applied within the optimized ranges to obtain the IN 625 material with maximum densification degrees and minimum defects by using Lasertec 30 SLM equipment.
9. I have demonstrated by computational and experimental methods that the IN 625 material manufactured by the SLM method is characterized, in both as-printed and heat-treated state, by a strong microstructural anisotropy that influences the mechanical tensile strength.
10. I have shown, based on the mechanical test performed for IN 625 manufactured using two scanning strategies and three building orientations that the specimens manufactured in vertical position

have the lowest mechanical tensile strengths regardless of the scanning strategy applied. However, the additive manufactured material using Lasertec 30 SLM equipment exceeds both standard specifications with the minimum requirements for both conventional and additive manufactured material.

11. I have conducted experimental research regarding the influence of high temperature exposure influence on additively manufactured IN 625, and the material's behavior was analyzed after exposure. The selected temperatures were similar to those in which the material operates (components of gas turbine engines). The research on the influence of isothermal oxidation on the material's characteristics is a topic of interest for the international scientific community and has been conducted originally. The results obtained showed that there are no significant differences between the behavior of the additive manufactured material and that of the manufactured by conventional methods.

The original results and contributions obtained in the thesis were used to write scientific papers that have been / will be published in specialized journals. Also, the research results were disseminated in scientific events.

The results obtained during this thesis are considered input data for future researches to fathom the knowledge in the field of additive manufactured metallic materials and in the field of additive manufacturing of components characterized by complex geometry that operate under severe conditions.

DISSEMINATION OF RESULTS

The dissemination of the research results carried out during the Ph.D. was achieved by publishing scientific papers in specialized journals and by participating in scientific communications.

Published papers in ISI ranked journals

1. **CONDRUZ M.R.**, MATACHE G., PARASCHIV A., BADEA T., BĂDILIȚĂ V., High temperature oxidation behavior of Selective Laser Melting manufactured IN 625, Metals 2020, 10, 668, ISSN 2075-4701, 2020 (impact factor 2,259)
2. **CONDRUZ M.R**., MATACHE G., PARASCHIV A., PUSCASU C., „Homogenization heat treatment and segregation analysis of equiaxed CMSX-4 superalloy for gas turbine components", Journal f Thermal Analysis and Calorimetry, Vol. 134, Issue 1, pp. 443-453, Springer Netherlands, 2018 (impact factor 2.471)

Published papers in ISI indexed journals

1. **CONDRUZ M.R.,** MATACHE G., PARASCHIV A., Characterization of IN 625 recycled powder used for selective laser melting, Manufacturing Review, Vol. 7, 5, 2020,
2. **CONDRUZ M.R**., MATACHE G., PARASCHIV A., Computational and experimental microstructure characterization of Selective Laser Melted IN 625 –UPB Scientific Bulletin, Series B, Vol 82, Issue 2, 2020
3. MATACHE G., VLADUT M., PARASCHIV A., **CONDRUZ M.R**., Edge and corner effects in selective laser melting of IN 625 alloy, Manufacturing Review, Vol. 7, 8, 2020, https://doi.org/10.1051/mfreview/2020008
4. **CONDRUZ M.R**., DUMITRESCU O., FRIGIOESCU T., CARLANESCU R., DUMITRU C., GHINEA A., Solidification Simulation and Casting of an Impeller Designed for a Thermochemical Treatment Furnace – accepted for publication in AIP Conference Proceedings at 05.09.2020

Published papers in international database indexed journals

1. **CONDRUZ M.R**., PARASCHIV A., PUȘCAȘU C., Heat treatment influence on hardness and microstructure of ADAM manufactured 17-4 PH, Scientific Journal Turbo, Vol. 5, nr. 2, ISSN 2559-608X, ISSN-L 1454-2897, 2018

2. MATACHE G., PARASCHIV. A., PUȘCAȘU C., **CONDRUZ R**., Simulation Segregation in CMSX-4 Superalloy: Experiments and Simulation Predictions, Scientific Journal Turbo, Vol. 4, nr. 1, pp. 11-14, ISSN 2559-608X, ISSN-L 1454-2897, 2017

Papers presented at conferences

1. 4th Central and Eastern European Conference on Thermal Analysis and Calorimetry, 28-31 August 2017, Chisinau, Moldova – poster session: **CONDRUZ M.R**., MATACHE G., PARASCHIV A., PUSCASU C. "Homogenization Heat Treatment and Segregation Analysis of Equiaxed CMSX-4 Superalloy for Gas Turbine Components"
2. The 1st International Conference on Emerging Technologies in Materials Engineering – EmergeMAT, 14-16 november 2018, Bucharest, Romania –poster session: PARASCHIV A., MATACHE G. **CONDRUZ M.R**. "Effect of laser scanning speed on microstructure and mechanical properties of selective laser melted Inconel 625"
3. 11th International Conference on Materials Science and Engineering, BRAMAT 2019, 13-16 march 2019 –poster session: CONDRUZ M.R., MATACHE G., PARASCHIV A. "Properties evaluation of SLM Manufactured Inconel 625"
4. The 2nd International Conference on Emerging Technologies in Materials Engineering – EmergeMAT, 6-8 november 2019, Bucharest, Romania - **CONDRUZ M.R.,** MATACHE G., PARASCHIV A. "Characterization of IN 625 Recycled Metal Powder used for Selective Laser Melting; MATACHE G., VLADUT M., PARASCHIV A., **CONDRUZ M.R**. Edge and corner effects in selective laser melting of IN 625 alloy
5. 12th Conference of the Euro-American Consortium for Promoting the Application of Mathematics in Technical and Natural Sciences – AMiTaNS 20, 24-29 June 2020, Albena, Bulgaria - **CONDRUZ M.R**., DUMITRESCU O., FRIGIOESCU T., CARLANESCU R., DUMITRU C., GHINEA A., „Solidification Simulation and Casting of an Impeller Designed for a Thermochemical Treatment Furnace"

In addition to the works carried out using the research results, during the Ph.D. other scientific papers in the field of materials science were made and published.

Published papers in ISI ranked journals

1. **CONDRUZ M.R**., PUSCASU C., VOICU L.R., VINTILA I.S., PARASCHIV A., MIREA D.A., „Fiber reinforced composite materials for proton radiation shielding", Materiale Plastice, Vol. 55, no. 1, 2018, (impact factor 1.248)
2. **CONDRUZ M.R**., VINTILAS.I., PARASCHIV A., PUSCASU C., DUMITRU F., Mechanical Property Evolution of Polymeric Composite Immersed in Jet Fuel, Acta Physica Polonica A, Vol. 135, No.5, pp. 965-967, 2019, (impact factor 0.556)
3. MIHALACHE R., **CONDRUZ M.R**., VINTILA I.S., VILAG V., STANCIU V., Centrifugal rotor blade: design and manufacturing using advanced composites, Revista de Materiale, no. 4, 2018 (impact factor 0,661)
4. **CONDRUZ M.R.**, MALAEL I., VINTILA I.S., PUSCAS CERNAT M, Manufacturing of advanced composite wind turbine blades for counter rotating vertical wind turbine, Materiale Plastice, Vol 57, Issue 2, 2020 (impact factor 1.393).

Published papers in ISI indexed journals

1. **CONDRUZ M**., PARASCHIV A., PUSCASU C., VINTILA I.S., „Tensile behavior of humid aged advanced composites for helicopter external fuel tank development", MATEC Web of Conferences, Vol. 155, 2018, https://doi.org/10.1051/matecconf/201814502004

Published papers in international database indexed journals

1. **CONDRUZ M.R**., VOICU L.R., PUSCASU C., VINTILA I.S., SIMA M., DEACONU M., DRAGASANU L., „Composite material designs for lightweight space packaging structures”, Vol. 10, Issue 1, pp. 13-25, 2018, DOI: 10.13111/2066-8201.2018.10.1.3
2. **CONDRUZ M.R**., PARASCHIV A., VINTILA I.S., SIMA M., DEUTSCHLANDER A., DUMITRU F., Evaluation of Low Velocity Impact Response of Carbon Fiber Reinforced Composites, Key Engineering Materials, Vol. 779, pp. 3-10, 2018, ISSN: 1662-9795, doi:10.4028/www.scientific.net/KEM.779.3
3. **CONDRUZ M.R.,** PARASCHIV A., DEUTSCHLANDER A., MINDRU I., "Assessment of GFRP Mechanical Properties in Order to Determine Suitability for UAV Components", Key Engineering Materials, pp. 57-66, 2020, doi:10.4028/www.scientific.net/KEM.834.57
4. **CONDRUZ M.R**., VINTILĂ I.S., „Carbon Nanotube and Nanoclay Based Polymeric Composites – Recent Achievements and Future Development Directions”, Scientific Journal Turbo, Vol. 4, nr. 1, pp. 19-22, ISSN 2559-608X, ISSN-L 1454-2897, 2017
5. **CONDRUZ M.R.**, VINTILA S., PARASCHIV A., „Evaluation of mechanical properties of carbon nenotube reinforced composites”, Scientific Journal Turbo, Vol. 4, nr. 2, pp. 19-24, ISSN 2559-608X, ISSN-L 1454-2897, 2017
6. VINTILA I.S., **CONDRUZ M.R**., SANDU C., SERBESCU H., On the Development of a Space Satellite Mirror with Intrinsic Self-Healing Properties, Materials Science Forum, Vol. 962, pp. 194-201 doi:10.4028/www.scientific.net/MSF.962.194
7. SIMA M., **CONDRUZ M.R.**, STĂNICĂ C., „Calculation of the Delamination Yield Index”, Jurnalul Științific Turbo, Vol. 4, no. 1, pp. 15-18, ISSN 2559-608X, ISSN-L 1454-2897, 2017
8. VINTILA S, **CONDRUZ R.**, PARASCHIV A, „Self-healing efficiency for fiber reinforced polymer composites”, Jurnalul Științific Turbo, Vol. 4, no. 2, pp. 14-18, ISSN 2559-608X, ISSN-L 1454-2897, 2017
9. FRIGIOESCU T.F., **CONDRUZ M.R.,** PARASCHIV A., BADEA T.A., ZAMFIR L.C., IONICA I., System and method designed for TBC Degradation Detection, Scientific Journal Turbo, Vol. 7, no. 1, 2020, pp. 73-78
10. BADEA T.A., PARASCHIV A., **CONDRUZ M.R**., FRIGIOESCU T.F., ZAMFIR L.C., IONICA I., Isothermal oxidation behavior and thermal shock resistance of thermal barrier coatings, Scientific Journal Turbo, Vol. 7, no. 1, 2020, pp. 65-72
11. FRIGIOESCU T.F., PARASCHIV A., **CONDRUZ M.R.,** BADEA T.A., ZAMFIR L.C., IONICA I., Finite Element Analysis on Temperature distribution of Thermal Barrier Coatings, Scientific Journal Turbo, Vol. 7, no. 1, 2020, pp. 101-107

Published papers in conference proceedings

1. VINTILĂ I.S., **CONDRUZ M.R**. FUIOREA I., MĂLĂEL I., SIMA M., Composite Wind Turbine Blade using Prepreg Technology, 6th CEAS Conference Proceeding (Ed. B. Gherman), pp. 5-14, 2017, ISBN: 978-973-0-25597-3

BIBLIOGRAPHY

Selective bibliography

[0] Wohlers Report 2019, Wohlers Associates, Colorado, USA, 2019

[97] J.A. Gonzalez, J. Mireles, S.W. Stafford, M.A. Perez, C.A. Terrazas, R.B.Wicker, Characterization of Inconel 625 fabricated using powder-bed-based additive manufacturing technologies, Journal of Materials Processing Technology, 264, https://doi.org/10.1016/j.jmatprotec.2018.08.031, 2019, pp. 200-210

[98] ASTM F3056-14, Standard Specification for Additive Manufacturing Nickel Alloy (UNS N06625) with Powder Bed Fusion

[121] J.H. Tan, W.L.E. Wong, K. W. Dalgarno, An overview of powder granulometry on feedstock and part performance in selective laser melting process, Additive Manufacturing, 18, https://doi.org/10.1016/j.addma.2017.10.011, 2017, pp. 228-255

[126] G. jacob, C. Brown, A. Donmez, S. Watson, J. Slotwinski, Effecs of powder recycling on stanless steel powder and built material properties in metal powder bed fusion processes, NIST Advanced Manufacturing Series 100-6, https://doi.org/10.6028/NIST.AMS.100-6, 2017

[129] H.P. Tang, M. Qian, N. Liu, X.Z. Zhang, G.Y. Yang, J. Wang, Effect of Powder Reuse Times on Additive Manufacturing of Ti-6Al-4V by Selective Electron Beam Melting, JOM, 67, https://doi.org/10.1007/s11837-015-1300-4, 2015, pp. 55-563

[216] G. Matache, D.M. Stefanescu, C. Puscasu, E. Alexandrescu, A. Buhrig-Polaczek, Investigation of solidification microstructure of single crystal CMSX-4 supralloy – experimental measurements and modelling predictions, International Journal of Cast Metals Research, 28 (6), http://dx.doi.org/10.1179/1743133615Y.0000000021, 2015, pp. 323-336

[236] SR EN ISO 3369 - Materiale metalice sinterizate impermeabile si aliaje dure sinterizate. Determinarea Densitatii

[239] ASTM B443 – Standard Specification for Nickel-Chromium-Molybdenum-Columbium Alloy and Nickel-Chromium-Molybdenum-Silicon Alloy Plate, Sheet, and Strip

[240] P.E. Carrion, A. Soltani-Tehrani, N. Phan, N. Shamsaei, Powder Recycling Effects on the Tensile and Fatigue Behavior of Additively Manufactured Ti-6Al-4V Parts, JOM, 71 (3), https://doi.org/10.1007/s11837-018-3248-7, 2019, pp. 963-973

[241] J.A. Slotwinski, E.J. Garboczi, P.E. Stutzman, C.F. Ferraris, S.S. Watson, M.A. Peltz, Characterization of Metal Powder Used for Additive Manufacturing, Journal of Research, http://dx.doi.org/10.6028/jres.119.018, 2014, pp.460-493

[247] M.J. Cieslak, T.J. Headley, T. Kollie, A.D. Romig Jr., A Melting and Solidification Study of Alloy 625, Mettalurgical Transactions A, 19A, 1988, pp. 2319-2331

[251] J.N DuPont, Solidification of an Alloy 625 Weld Overlay, Metallurgical and Materials Transactions A, 27A, 1996, pp. 3612-3620

[252] S. Barella, A. Gruttadauria, C. Mapelli, D. Mombelli, P. Taiana, M. Bosatra, A. Morini, Solidification microstructure of centrifugally cast Inconel 625, China Foundry, 14 (4), DOI: 10.1007/s41230-017-7017-y, 2017, pp. 304-312

[254] Y. Gao, M. Zhou, Superior Mechanical Behavior and Fretting Wear Resistance of 3D-Printed Inconel 625 Superalloy, Applied Sciences, 8 (12), https://doi.org/10.3390/app8122439, 2018,2439

[255] T. Terris, F. Adamski, P. Peyre, C. Dupuy, Influence of SLM process parameters on Inconel 625 superalloy samples, Proceedins of Lasers in Manufacturing Conference 2017, Munchen, Germany, 2017 https://www.wlt.de/lim/Proceedings2017/Data/PDF/Contribution110_final.pdf

[257] D.M. Stefanescu, Cresterea celulara si dendritica, in Stiinta si Ingineria solidificarii pieselor turnate, Ed. Agir, 2007, pp. 207-258

[259] Heat Treater's Guide, Practices and Procedures for Nonferrous Alloys, H. Chandler Ed., ASM, Materials Park, Ohio, 1996, pp. 88-97

[260] F. Tehovnik, J. Burha, B. Podgornik, M. Godec, F. Vode, Microstructural evolution of Inconel 625 during hot rolling, Materials and technology, 49(5), doi:10.17222/mit.2015.274, 2015, pp. 801-806

[261] K. Amato, J. Hernandez, L. Murr, E. Martinez, S. Gaytan, P.W. Shindo, Comparison of Microstructures and Properties for a Ni-Base Superalloy (Alloy 625) Fabricated by Electron and Laser Beam Melting, Journal of Materials Science Research, 1(2), http://dx.doi.org/10.5539/jmsr.v1n2p3, 2012, pp. 3-41

[262] M.A. Anam, Microstructure and mechanical properties of selective laser melted superalloy Inconel 625, Electronic Theses and Dissertation, Paper 3029, University of Louisville, 2018

[263] M.R. Condruz, G. Matache, A. Paraschiv, T. Badea, High Temperature Oxidation Behavior of Selective Laser Melting Manufactured IN 625, Metals, 2020, 10, 668, doi:10.3390/met10050668

[264] Y.J. Kang, S. Yang, Y.K. Kim, B. AlMangour, K.A. Lee, Effect of post-treatment on the microstructure and high-temperature oxidation behaviour of additively manufactured Inconel 718 alloy, Corrosion Science, 158, https://doi.org/10.1016/j.corsci.2019.06.030, 2019, 108082

[265] H. Buscail, R. Rolland, C. Issartel, F. Rabaste, F. Riffard, L. Aranda, M. Vilasi, Effects of water vapour on the oxidation of a nickel-base 625 alloy between 900 and 1100°C, Journal of Material Science, 46, DOI 10.1007/s10853-011-5544-2, 2011, pp. 5903-5915

[266] A. Chyrkin, P. Huczkowski, V. Shemet, L. Singheiser, W.J. Quadakkers, Sub-Scale Depletion and Enrichment Processes During High Temperature oxidation of the Nickel Base Alloy 625 in the Temperature Range 900 - 1000°C, Oxidation of Metals, 75, DOI 10.1007/s11085-010-9225-3, 2011, pp. 143-166

[267] J. Colas, L. Charpentler, M. Balat-Pichelin, Oxidation in Air at 1400 K and Optical Properties of Inconel 625, FeCrAloy and Kanthal Super ER, Oxidation of Metals, 93, https://doi.org/10.1007/s11085-020-09959-6, 2020, pp. 355-370

[268] E. N'dah, M.P. Hierro, K. Borrero, F.J. Perez, Study of the Cyclic Oxidation Resistance of Superalloy IN-625: Lifetime Predicted by COSP-Modelling Program, Oxidation of metals, 68 (1/2), DOI 10.1007/s11085-006-9048-4, 2007, pp. 9-21

[270] L. Kumar, R. Venkataramani, M. Sundararaman, P. Mukhopadhyay, S.P. Garg, Studies on the Oxidation Behavior of Inconel 625 Between 873 and 1523 K, Oxidation of Metals, 45, https://doi.org/10.1007/BF01046827, 1996, pp. 221–244.

[271] A. Encinas-Orpesa, G.L. Drew, M.C. Hardy, A.J. Leggett, J.R. Nichollas, N.J. Simms, Effects of Oxidation and Hot Corrosion in a Nickel Disc Alloy, in Superalloys 2018; Reed, R.C., Green, K.A., Caron, P., Gabb, T.P., Fahrmann, M.G., Huron, E.S., Woodard, S.A. Ed.; TMS: Pittsburg, Pennsylvania, 2008, pp. 609–618

[277] H. Kitaguchi, Microstructure-Property Relationship in Advanced Ni-Based Superalloys, In Metallurgy–Advances in Materials and Processes; Y. Pardhi, Ed., IntechOpen: Rijeka, Croatia, http://dx.doi.org/10.5772/2852, 2012; pp. 19–42.

[278] D.M. Gorman, R.L. Higginson, H. Du, G. McColvin, A.T. Fry, R.C. Thomson, Microstructural Analysis of IN617 and IN 625 Oxidised in the Presence of Steam for use in Ultra-Supercritical Power Plant, Oxidation of Metals, 79, https://doi.org/10.1007/s11085-012-9342-2, 2013, pp. 553–566